A METHOD FOR MONOCHROMATIZATION AND PRECISE POINT FOCUSING OF X-RAYS AND ITS APPLICATION IN LOW ANGLE DIFFRACTION STUDIES

Thesis by

Dwight Winton Berreman

In Partial Fulfillment of the Requirements

for the Degree of

Doctor of Philosophy

California Institute of Technology

Pasadena, California

1955

ACKNOWLEDGEMENTS

I wish to express my sincere appreciation to Dr. Jesse W.M. DuMond for his enthusiastic support and his patience in advising me during my research.

I also wish to thank Mr. Robert L. Shacklett for helping me to start in the field of low angle x-ray diffraction.

I appreciate the suggestions and cooperation, which I received from several members of the other departments, in obtaining materials for study with the new instrument.

Finally, I am grateful to my wife and my parents for their help and encouragement during my studies and research.

The project was sponsored in part by the Office of Naval Research, and in part by the Atomic Energy Commission.

ABSTRACT

A principle for bending crystals with a minimum of strain so that they will focus x-rays and γ-rays accurately to a point is explained.

Detailed calculations are made of the aberrations in the foci resulting from various applications of the principle.

The application of the principle in making a point focusing monochromator for low angle x-ray diffraction studies is discussed, and theoretical and experimental determinations of the reflection coefficient of the crystal are compared.

A few experiments in low angle diffraction from biological materials using the new monochromator are described, and the results are compared with those obtained using other instruments.

Table of Contents

Table of Contents

I X-RAY FOCUSING WITH DOUBLY CURVED CRYSTALS

Crystal reflection has long been recognized as a valuable tool for simultaneously collimating and spectrally resolving beams of x-rays and γ-rays. The degree of spectral resolution and collimation depends greatly on the degree of perfection of the crystal lattice structure.

The work to follow is intended to illustrate the applications and advantages of a method whereby a single crystal with very perfect lattice structure may be bent, without seriously disturbing the lattice structure of the crystal, in such a way as to deflect certain wave-lengths of an impinging beam of x-rays or γ-rays so that they will converge toward a point.

One important application of such a point focusing crystal is in the formation of a converging monochromator beam for use in studying the low angle x-ray diffraction patterns of submicroscopic particles.

1. Properties of Crystal Reflection

A curved crystal may be used to reflect and focus x-rays from its curved atomic planes in much the same manner as light is focused by reflection from curved mirrors. If the curved crystal is ideally perfect, i.e., if there are no local irregularities in the crystal lattice structure, the reflected x-rays will obey the laws of geometrical optics to an extremely high degree of accuracy because the x-ray wave-lengths are much smaller than the dimensions of the uniform regions

of the atomic planes from which the rays are reflected. However, if the curved crystal is mosaic, i.e., if it has many local irregularities in its lattice structure, the regions over which the atomic planes have no discontinuities may be so small that the diffraction effects are an important consideration in the focusing properties of the crystal, just as they are when very small apertures are used in focusing light. It is also frequently the case that the angular disorientation in the crystallites or domains of a mosaic crystal are sufficiently large to have a serious effect on its focusing properties.

It has been shown theoretically that there is a slight difference between the angle of incidence and the angle of reflection of x-rays from atomic planes (1), but the difference is too small to be of practical importance in our calculations.

The main practical difference between reflection of light from mirrors and reflection of x-rays from atomic planes of crystals is that the reflection coefficient for x-rays of any one layer of atoms in a crystal is extremely small, so that interference effects between the x-rays reflected from the various uniformly spaced parallel crystal planes allow appreciable reflection of only one very narrow band of wave-lengths in each order of reflection from any one angle of incidence. The approximate wave length of this band is given by Bragg's law (2)

$$n\lambda = 2d \sin \theta \qquad \text{(I-1.1)}$$

where d is the space between the parallel atomic planes, or Bragg planes, θ is the angle between the propagation vector of the incident or reflected beam and the atomic planes, and n is the order of the

reflection, and hence, an integer.

Darwin (3) and Ewald (4) have derived expressions for the relation between the fraction of x-rays of a given wave-length that will be reflected from ideally perfect crystals, and the angle of incidence of the beam. The fraction is negligible except over extremely narrow angular bands. Their equations may be manipulated to obtain the width of the band of wave-lengths that are appreciably reflected at a particular angle.

The narrowness of the angular band makes it possible to use crystals to select and focus almost pure monochromatic radiation at an image point of a bent crystal, although it seriously limits the proportion of the total x-ray flux from a polychromatic source that may be reflected toward that image point.

2. The First Solutions to the Point Focusing Problem

The problem of obtaining an exact point image from a point source of monochromatic radiation by Bragg reflection from a single large crystalline lamina appears to have only one type of solution (Fig. I-1.1). In any plane containing the source and image points, P_1, P_2, the surface, S, of the lamina, L, must lie on a circle through the two foci, P_1, P_2, while the Bragg planes, B, must be curved so as to be concentric around a point, A, on the circle half way between the two foci. This two dimensional part of the solution was first suggested by DuMond and Kirkpatrick (5) in 1930, but was first actually realized by Johansson (6) in 1932.

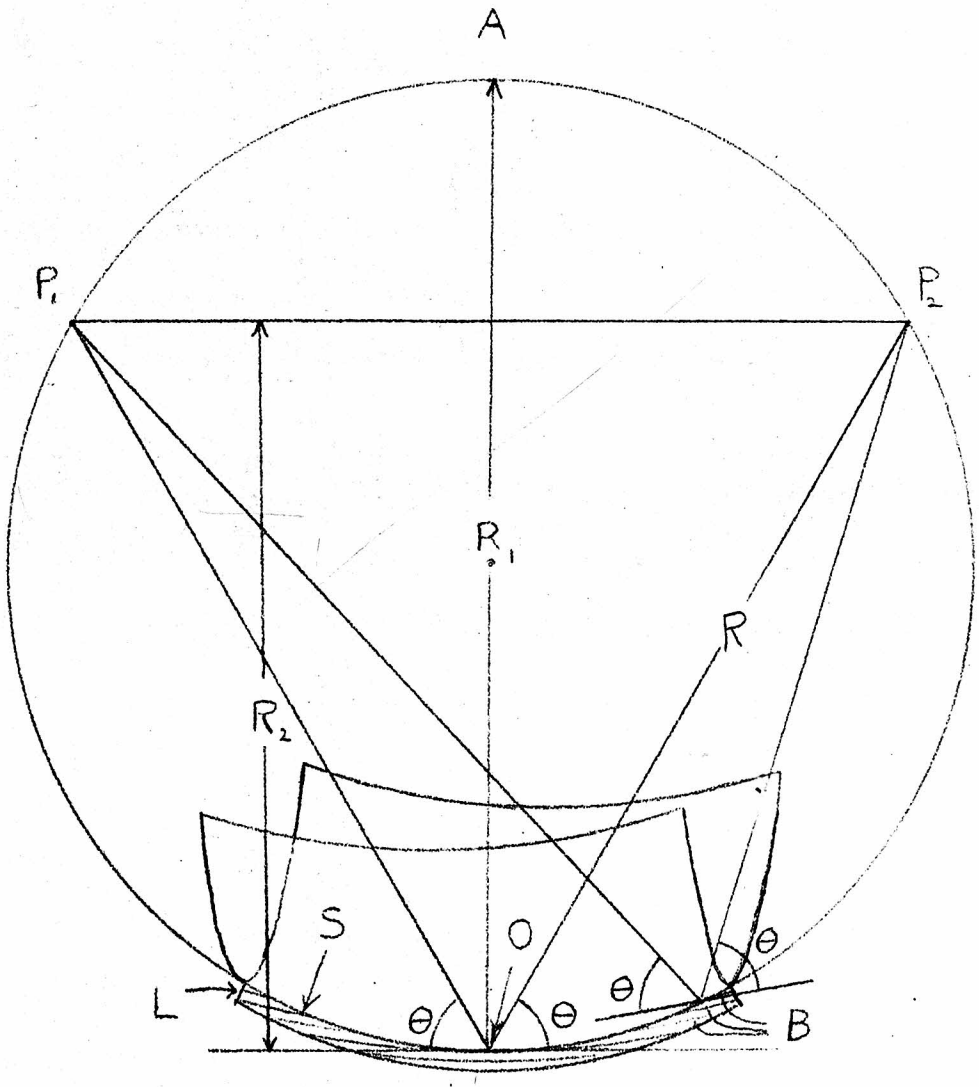

Fig. I-1.1 Geometry for focusing monochromatic x-rays exactly from P_1 to P_2.

L = crystal lamina in the shape of a segment of a toroid.

S = concave crystal surface.

B = Bragg planes.

In the intervening year, 1931, H.H. Johann (7) approximated the geometry (Fig. I-1.1) by bending a flat lamina of mica to the appropriate radius, R_1.

Since that time, several people and groups (8,9) have extended this principle from line focusing to point focusing by using crystals, such as aluminum and lithium fluoride, which may be plastically deformed into a toroidal figure of revolution about the line $\overline{P_1P_2}$ (Fig. I-1.1). If R is the chord from either focus to the center of symmetry, O, where the crystal planes are tangent to the focal circle, then this length, R, is related to the two principal radii of curvature, R_1 and R_2, of the crystal planes at O by the relation:

$$R_2 = R \sin\theta = R_1 \sin^2\theta \qquad \text{(I-1.2)}$$

where θ is the Bragg angle.

For this three-dimensional geometry (Fig. I-1.1), plastic bending of the crystal has been used almost exclusively because the crystal lamina must be strained beyond its elastic limit to make the final lamina conform to the appropriate non-developable surface over reasonably large solid angles.

Plastic deformation of a crystal causes such severe disruption of its lattice structure that the focusing property of the crystal is somewhat impaired. Furthermore, the crystals that can be deformed in this way generally have rather imperfect crystal structure even before they are bent.

Attempts have also been made to approximate the above point-

focusing geometry by stretching a sheet of mica into a concavity with two principal radii of curvature by drawing the air out from behind the crystal. However, mica is an imperfect crystal even when it is unstressed, and the extreme strains introduced by this procedure seem to disrupt its structure still more, so that the resolution of such a crystal is very poor. Warren Danielson and Leon Shenfil have done unpublished work on this system at the California Institute of Technology, but it has not given a satisfactorily sharp focus for low angle diffraction work thus far.

Hence, for use in point focusing monochromators for low angle diffraction studies, and in spectrometers, it seems preferable, and indeed necessary, because of the sharp focusing required, to use elastically bent crystals of materials, such as quartz, which have nearly perfect lattice structure.

II BENDING LAMINAE WITH DEVELOPABLE SURFACES

Although exact point-to-point focusing of x-rays of one wave-length over large solid angles by elastically bent crystals may be impossible, it is possible to obtain geometrically exact line-to-point focusing of a single wave-length; good approximate point-to-point focusing of a single wave-length; or exact point-to-point focusing of a narrow band of wave-lengths with elastically bent crystals by the method to be described.

For convenience of description, an imaginary surface half way between the two real, parallel surfaces of a thin crystal lamina will be called its mid-surface.

Since the strains in a thin bent lamina are approximately proportional to the distance from its neutral or unstressed surface, a lamina in which the midsurface and neutral surface always coincide has less maximum strain for a given curvature than if the two surfaces do not coincide everywhere.

Hence, if a crystal lamina is to be bent so that certain Bragg planes are given two principal radii of curvature, the radii may be made shortest relative to the thickness of the lamina if the bending is done in such a way that the mid-surface is always a neutral surface. This will be the case if the mid-surface is always a developable surface. Two principal radii of curvature may be introduced in the Bragg planes by starting with a cylindrical or conical lamina of unstressed crystal in which the Bragg planes are flat, flattening this lamina so that the Bragg planes have one principal radius of curvature

at each point while the mid-surface is flat, and then bending the lamina into some other cylinder or cone whose axis is not parallel to that of the original curve. Fig. II-1.1 is the illustration from a letter to the editor published in the Review of Scientific Instruments, (10) illustrating this bending process as it was applied in the construction of a point focusing monochromator which will be described in more detail in Part VII.

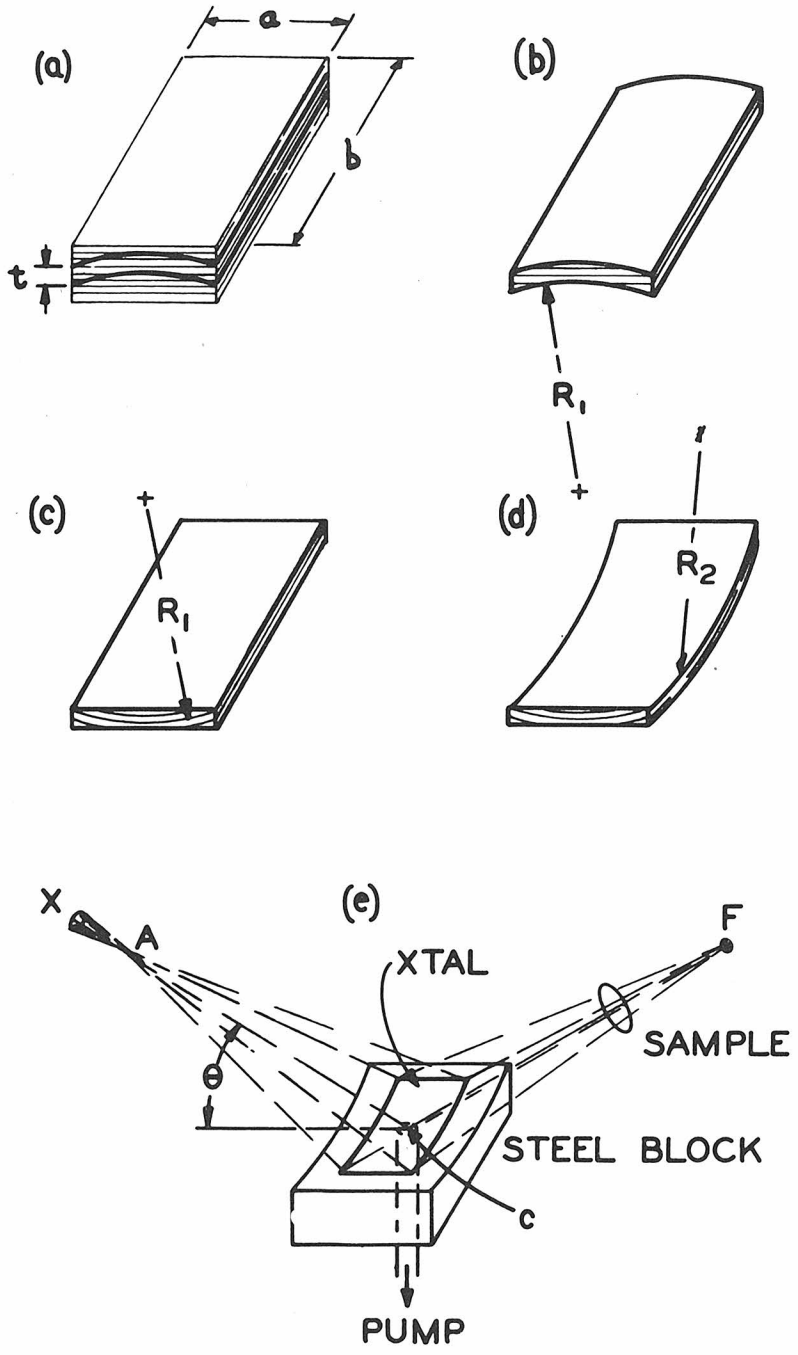

Fig. II - 1.1. Process of making a single-crystal monochromator.

(a) Original block of quartz:
a = 3.8 cm, b = 7.6 cm, t = 0.025 cm.

(b) Finished lamina: R_1 = 105 cm.

(c) Flattened lamina.

(d) Final shape: $R_2 = R_1 \sin^2\theta$ = 95 cm.

(e) Mounting and X-ray beam:
$\overline{AC} = \overline{CF} = R_1 \sin\theta$ = 100 cm, $\theta = 71^\circ 42'$.

III APPLICATIONS OF THE BENDING PRINCIPLE

1. The Problem

The first problem in the application of the principle of bending just described is to find the shape of the unstressed lamina, in which the Bragg planes are flat, required to give the desired double curvature to the Bragg planes when the lamina is bent to its final shape.

Since laminae in the form of segments of circular cylinders are much easier to make than other developable surface forms, the calculations of geometrically exact shapes for unstressed laminae will be followed by determinations of the aberration introduced by approximating these shapes with circular cylinders.

In the calculations, henceforth, it will be assumed that when the crystal lamina is bent flat it becomes a rectangle of width a, length b, and thickness t (Fig. III-1.1). Let us place an origin O at the center of the midsurface of the rectangular lamina, and attach to this origin and midsurface the coordinates x, y, and z. Let x always remain normal to the surface, and let the y and z coordinates bend to follow the midsurface, even when the midsurface is not flat. Let us also introduce the coordinate system, X, Y, and Z, which coincides with x, y, z at O but is always a straight, rectangular system (Fig. III-1.2).

A simple observation at this point will double the number of cases covered in the succeeding calculations. For every geometry

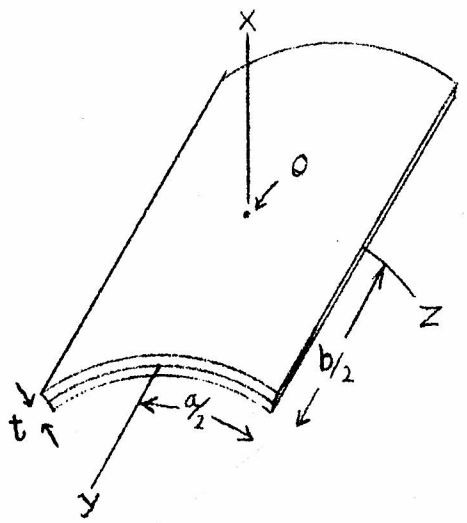

Fig. III-1.1 The x, y, z coordinate system in the unstressed crystal lamina. a = width. b = length. t = thickness. y and z lie on the midsurface of the lamina.

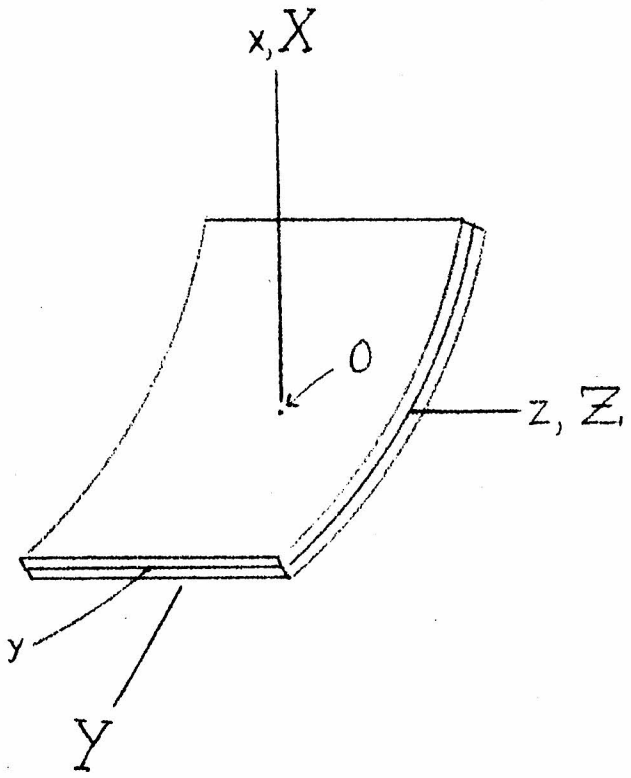

Fig. III-1.2 The x, y, z and X, Y, Z coordinate systems in the finally curved lamina.

involving two real foci, such as a real line and a real point, there is a similar geometry involving one real and one virtual focus. The crystal laminae for the two cases are bent in exactly the same way. The only difference is that in the two-real-foci case, the angle P_1-z-P_2 is bisected by the normal, N, to the Bragg planes (Fig. III-1.3). In the virtual-real-foci case, the Bragg planes, B, themselves bisect this angle, and the actual x-ray beam travels <u>through</u> the crystal lamina, L, (Fig. III-1.4). Thus, the crystals look the same for the two cases, but the Bragg planes in one case are at right angles to those in the other. The difference is the same as that between what are commonly called "transmission" focusing and "reflection" focusing in the case of singly curved crystals.

For simplicity, all calculations will be made for two real foci, or "reflection" focusing.

2. <u>Line-to-Point Geometry</u>

Now let us find an exact geometry for focusing all the x-rays of a given wave-length, λ, from the crystal to a point, F_2 (Fig. III-2.1) which will be called the normal focus, with coordinates (R_2, 0, 0) in the X, Y, Z system. Let us assume that the band of wave-lengths that may be reflected at one angle, θ, is of negligible width.

Suppose the final lamina has its midsurface bent to a circular cylinder of radius R_2 around the axis $X = R_2$, $Y = 0$, which shall be called the f-axis hereafter, and let the source lie in a line along

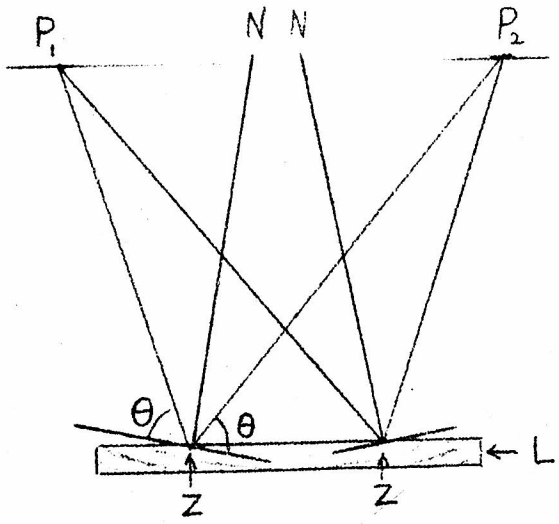

Fig. III-1.3 Reflection geometry.
z = points of reflection.
N = normals to Bragg planes.
L = crystal lamina.
P_1 and P_2 = real foci.
θ = Bragg angle at z.

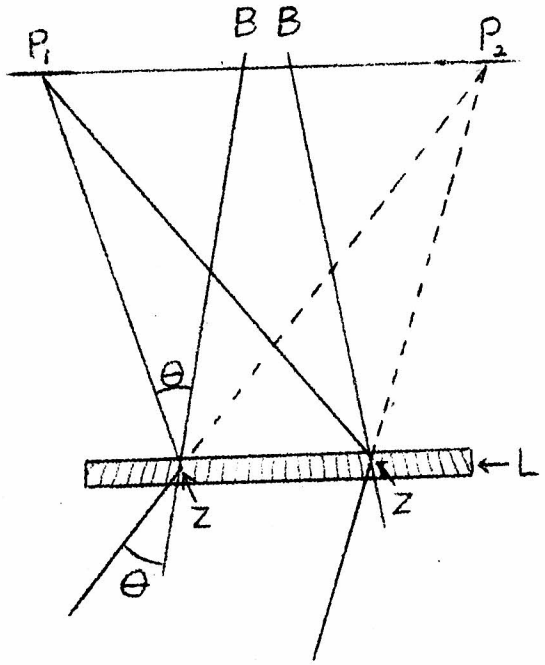

Fig. III-1.4 Transmission geometry.
z = points of deflection.
B = extensions of the Bragg planes.
L = crystal lamina.
P_1 = real focus.
P_2 = virtual focus.

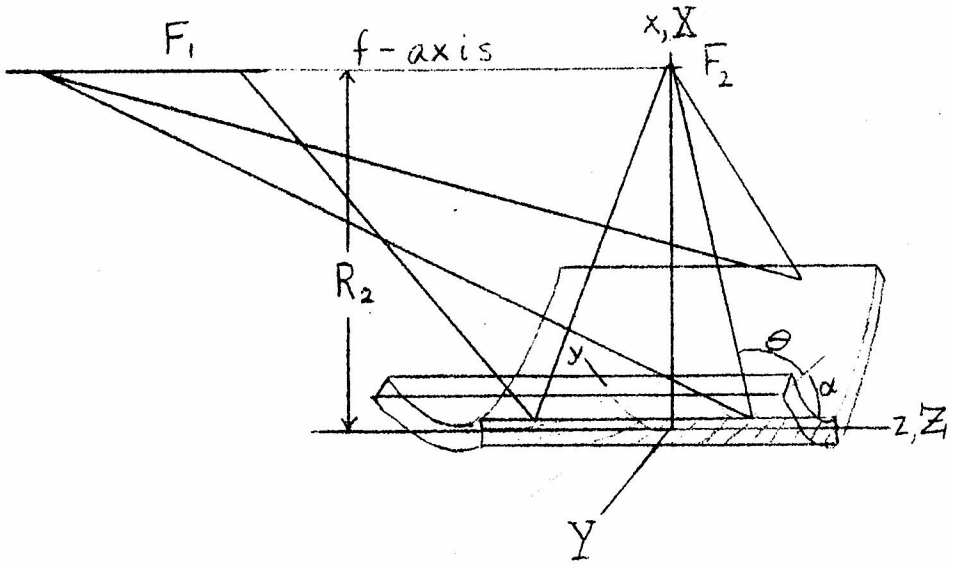

Fig. III-2.1 A cylindrical crystal bent to focus a monochromatic beam of x-rays toward a point, F_2, from a line, F_1.
α = angle between Bragg planes and crystal surface.
θ = Bragg angle.
f-axis = focal axis, and the axis of the final cylinder.
R_2 = radius of final cylinder.

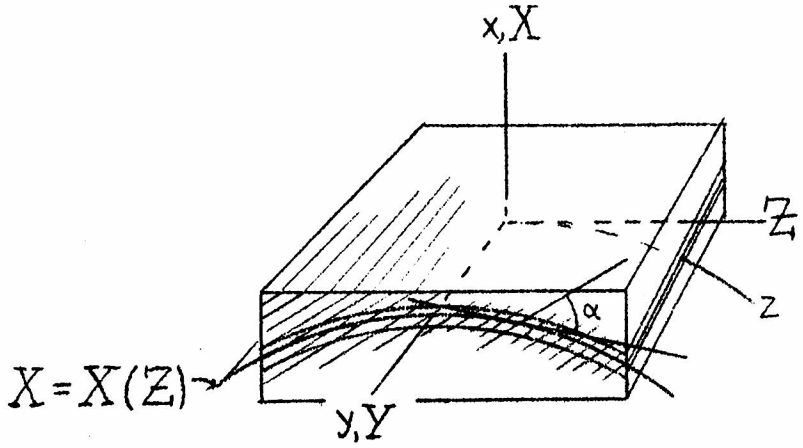

Fig. III-2.2 The unstressed cylinder for perfect monochromatic focusing, superimposed on the crystal block from which it is cut. $X = X(Z)$ is the equation of the midsurface of the unstressed lamina.

the f-axis. Then we may see by symmetry that the Bragg planes should have orientations in the lamina which depend on z but not on y. If the angle at which these Bragg planes cross the midsurface is called α, then $\alpha = \alpha(z)$.

Let us assume, for the present, that the thickness, t, is so small that no distinction need be drawn between the midsurface and other locations where x-rays might be reflected.

The condition $\alpha = \alpha(z)$ is equivalent to stating that the original unstressed lamina, in which the Bragg planes are flat, is a cylinder with straight axes parallel to the Y axis. It is not necessarily a circular cylinder. Notice that the condition requiring developable initial and final surfaces is satisfied.

The problem thus reduces to finding $\alpha(z)$, and from that finding the cross section shape of the unstressed cylinder: $X = X(Z)$ (Fig. III-2.2). In order to obtain a point focus at F_2 (Fig. III-2.1), the angle Θ must be the Bragg angle for the desired wave-length. As can be seen in Fig. III-2.1, the value of the angle α at $z = 0$ is $\alpha(0) = \frac{\pi}{2} - \Theta$. Elsewhere

$$\alpha(z) = \alpha(0) + \tan^{-1} \frac{z}{R_2} \qquad \text{(III-2.1)}$$

To find X(Z), we may write down two equations (examine Fig. III-2.2):

$$Z(z) = \int_0^z \cos(\alpha - \alpha(0))dz = \int_0^z \cos(\tan^{-1} \frac{z}{R_2})\, dz \qquad \text{(III-2.2)}$$

$$= R_2 \sinh^{-1} \frac{z}{R_2}$$

and

$$X(z) = -\int_0^z \sin(\alpha-\alpha(0))dz = x_0(1-\sqrt{1+(z/R_2)^2} \qquad \text{(III-2.3)}$$

Solving for z in both equations gives

$$z = R_2 \sinh (Z/R_2) = R_2 \sqrt{\left(\frac{X}{R_2}+1\right)^2 - 1}$$

which reduces to

$$X(Z) = R_2(1-\cosh \frac{Z}{R_2}) \qquad \text{(III-2.4)}$$

Notice that the radius of curvature of X(Z) at Z = 0, which will be called $-R_1$, is in this case $-R_1 = -R_2$. When the lamina is flat or in its final shape, a Bragg plane that was originally flat and tangent to the surface at 0 would be given a radius of curvature equal to $+R_1$ upon flattening the lamina. In this geometry, then, $R_1 = R_2$.

Let us call the conjugate focus, F_1, the off-normal focus. It is not a point, but a line segment along $X = R_1$ in this geometry. The position of the intersection of a ray from a point z on the crystal with this focal line has a Z coordinate which we shall call $f_1(z)$. In general, F_2 need not be a fixed point, so let the Z coordinate of a ray through F_2 be $f_2(z)$. This geometry is a special case in which $f_2(z) \equiv 0$.

The quantities z/R_1, $f_1(z)/R_1$, and $f_2(z)/R_1$ appear so frequently that it is convenient to use coordinates in which R_1 is the unit of

length. We shall therefore introduce the dimensionless system.

$$u = z/R_1 , \quad v = f_1/R_1 , \quad w = f_2/R_1 \tag{III-2.5}$$

Let us now calculate the length, Δf_1, of the off-normal line focus of a crystal of width a, bent to give a perfect monochromatic focus at the point F_2, where F_2 is situated at $X = R_1$, $Y = 0$, $Z = 0$. Let $\beta(z)$ be the angle between a ray and the normal to the crystal surface at its point of incidence, z, as shown in Fig. III-2.3. Since we are only considering one wave-length, we must have

$$\beta(z) - \beta(0) = \alpha(z) - \alpha(0) \tag{III-2.6}$$

It was seen in Fig. III-2.1 that

$$\alpha(z) - \alpha(0) = \tan^{-1} \frac{z}{R_2}$$

Hence, in the u, v, w notation,

$$\beta(u) = \beta(0) + \tan^{-1} u$$

Referring to Fig. III-2.3 again, we may observe that

$$f_1/R_1 \equiv v = u - \tan \beta(u) = u - \tan(\beta(0) + \tan^{-1} u) \tag{III-2.7}$$

Unless the crystal is very wide, u will always be sufficiently small that an expansion of v in powers of u will converge fairly rapidly.

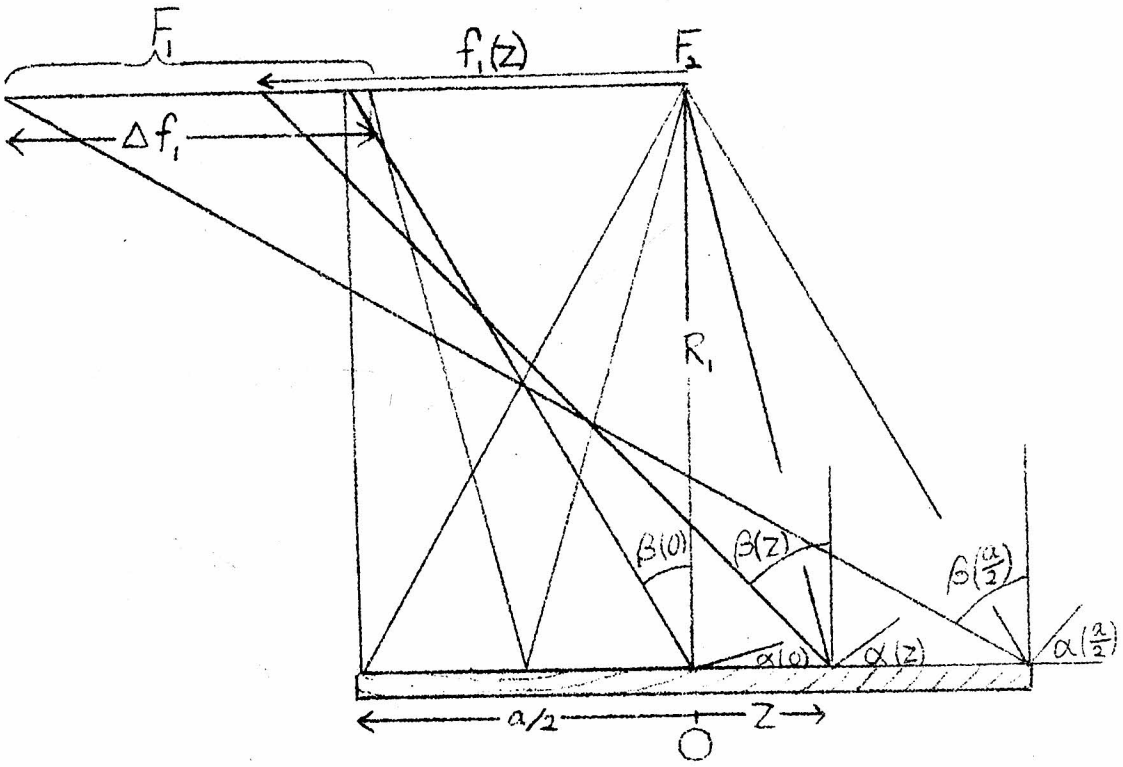

Fig. III-2.3 Geometry for perfect monochromatic line-to-point focusing.

F_1 = off-normal focus.
Δf_1 = length of off-normal focus
F_2 = normal focus.
$\alpha(z)$ = angle between crystal surface and Bragg planes.
$\beta(z)$ = angle between beam and crystal surface normal

Since

$$\tan(\beta + \epsilon) = \frac{\tan\beta + \tan\epsilon}{1 - \tan\beta\tan\epsilon} = (\tan\beta + \tan\epsilon)(1 + \tan\beta\tan\epsilon + \ldots)$$

$$= \tan\beta + (1+\tan^2\beta)(\tan\epsilon + \tan^2\epsilon\tan\beta + \tan^3\epsilon\tan^2\beta + \ldots)$$

(III-2.8)

we may write

$$v = u - \left[\tan\beta(0) + u(1 + \tan^2\beta(0)) + u^2\tan\beta(0)(1 + \tan^2\beta(0)) + \ldots\right]$$

or

$$v = -\left[\tan\beta(0) + u\tan^2\beta(0) + (1+\tan^2\beta(0))(u^2\tan\beta(0) + u^3\tan^2\beta(0) + \ldots)\right]$$

(III-2.9)

In the special case where $f_2(z) \equiv 0$, $\beta(0) = \pi - 2\theta$ for "reflection" type focusing, or $\beta(0) = 2\theta$ for "transmission" focusing. Hence, in this case, a crystal of width a has a conjugate focus of length

$$\Delta f_1 = a\tan^2 2\theta + \text{terms of order } a^2/R_1 \qquad \text{(III-2.10)}$$

3. Approximate Line-to-Point Geometry

The best approximation to any cylindrical surface, using a circular cylindrical segment, is the one where the center of the segment is at a point of zero rate of change in radius of curvature. For the $R_2(1 - \cosh\frac{Z}{R_2})$ cylinder, which, for simplicity, we shall call the cosh cylinder, this position is clearly the one of symmetry about

$Z = 0$ (Fig. III-3.1). If we let the radius of the approximating cylinder be $-R_1 = -R_2$ before it is flattened, then $\alpha(z) = \alpha(0) + z/R_1$, or $\alpha(u) = \alpha(0) + u$. Likewise, $\beta(u) = \beta(0) + u$.

Here, as in the perfect focusing case, it is clear from Fig. III-2.3 that $f_1/R_2 = v = u - \tan\beta(u)$, the only difference being that here $\beta(u) = \beta(0) + u$ rather than $\beta(0) + \tan^{-1} u$.

Using Eq. III-2.8 again, where ϵ now equals u rather than $\tan^{-1} u$, gives

$$v = u - \left[\tan\beta(0) + \tan u(1 + \tan^2\beta(0)) + \tan^2 u \tan\beta(0)(1 + \tan^2\beta(0)) + \ldots\right]$$

By expanding tan u in a series and rearranging terms, we obtain

$$v = -\left[\tan\beta(0) + u\tan^2\beta(0) + u^2\tan\beta(0)(1 + \tan^2\beta(0)) + u^3(\tan^2\beta(0) + \tfrac{1}{3})(1 + \tan^2\beta(0)) + \ldots\right] \qquad \text{(III-3.1)}$$

Notice that Eq. III-3.1 differs from Eq. III-2.4 only by the term $(u^3/3)(1+\tan^2\beta(0))$ and higher order terms in u. The effect of this term is of little consequence in the size of the off-normal focus, but the same expression applies to the approximate point focus, F_2. At that focus, $\beta(0) = 0$, and the added term gives an aberration: $w = u^3/3$. That is, for a crystal of width a, the "point focus" has a length

$$\Delta f_2 \approx R_1 \cdot \frac{2}{3}\left(\frac{a}{2R_1}\right)^3 = \frac{a^3}{12R_1^2} \qquad \text{(III-3.2)}$$

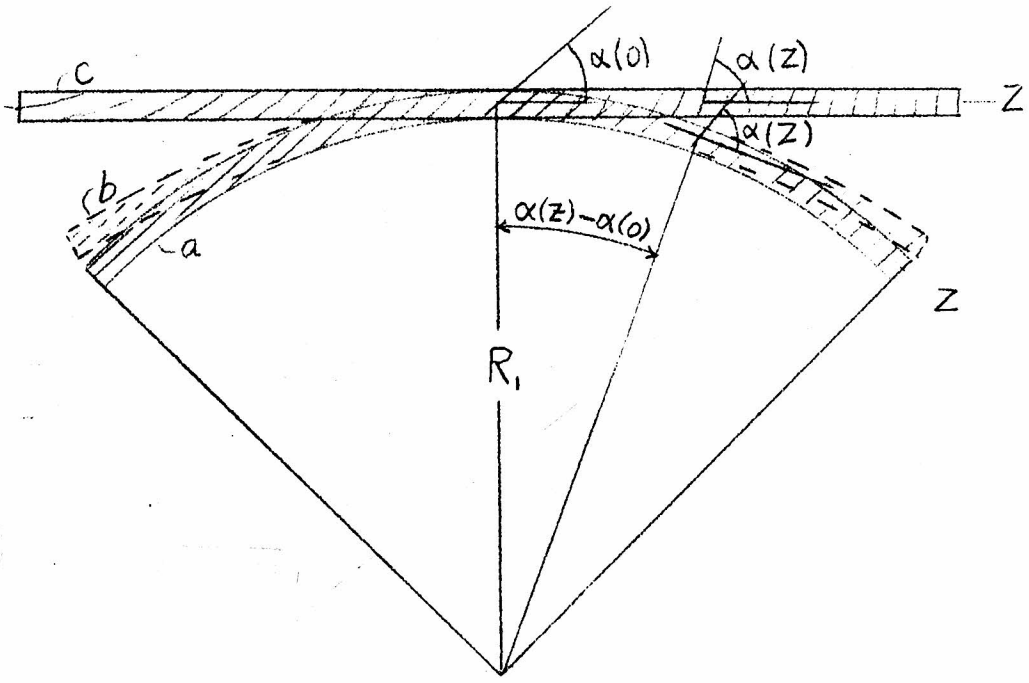

Fig. III-3.1 Illustration of the relation between the unbent crystal snape and the function $\alpha(z)$.

a = circular cylinder.
b = cosh cylinder.
c = flattened lamina.

Note that $\alpha(z) = z/R_1$ for a circular cylinder.

if the unstressed lamina is a circular cylinder rather than a cosh cylinder.

4. The Focal Circle

From the equations for f_1 just derived for both the cosh and the circular cylinders, we can see that for small u, the off-normal focus position is approximately $v = -(\tan\beta(0) + u \tan^2\beta(0))$.

By examining Fig. III-4.1, it can be seen that if lines are drawn through a point P_1 on a circle tangent to the crystal and to the f-axis, then $v(u) = -(\tan\beta(0) + u \tan^2\beta(0))$. Hence, this circle represents the locus of points at which the Z component of the spread of rays of a given wave-length from the crystal is of second order and higher in u. This circle will hereafter be called the focal circle. It may be noticed that this circle bears the same relation to the Bragg planes of the crystal as did the focal circle in the perfect focusing geometry of DuMond and Kirkpatrick (5) described in Part I. There would be no Z-aberration on this circle if the surface of the lamina followed the circle rather than being straight and tangent, and if the Bragg planes were circular cylinders concentric with the midpoint, on the circle, between the two foci.

Let us now draw a line parallel to the f-axis through P_1 and call it the p-axis. Let us also make the definition $p_1 \equiv Z/R_1$, where Z is the Z-coordinate of the intersection of a ray, from a position, u, on the crystal, with the p-axis (Fig. III-4.2). With this construction, we can find the exact position of the first focus, P_1, as a

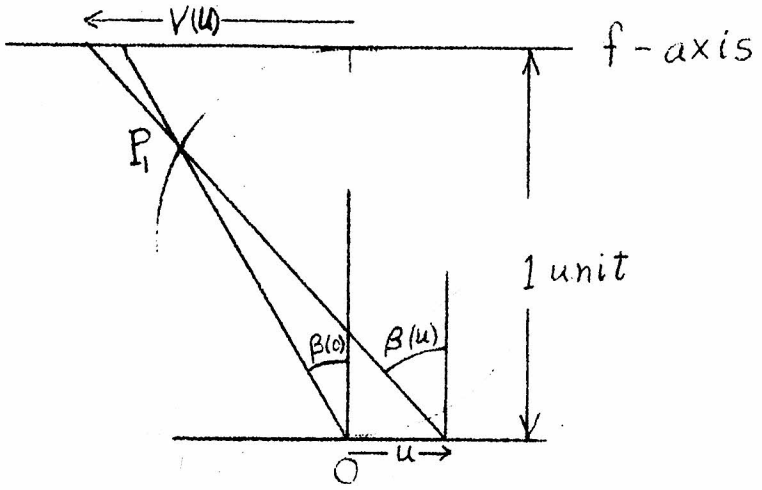

Fig. III-4.1 The focal circle in dimensionless units.

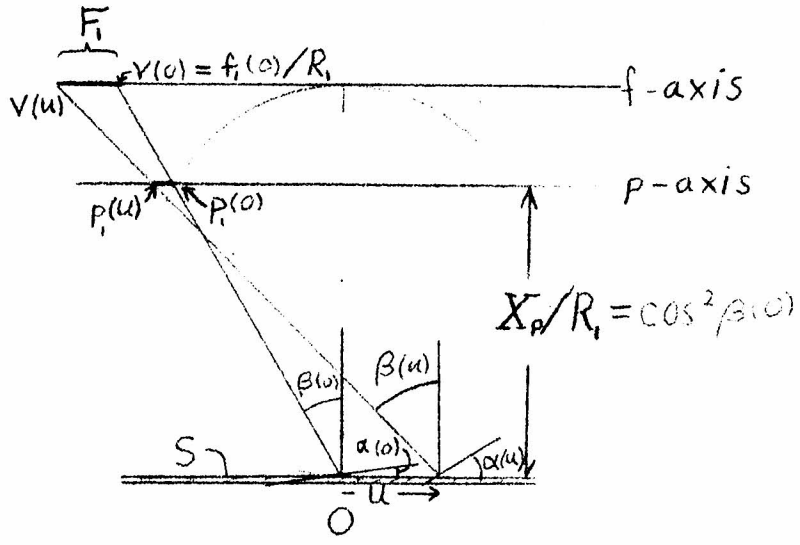

Fig. III-4.2 The focal circle, with aberrations, in dimensionless units.
S = crystal surface.

function of u. Let X_p be the X-coordinate of the p-axis. Then

$$p_1 = \frac{-X_p}{R_1} \tan\beta(u) + u \qquad \text{(III-4.1)}$$

But the geometry of Fig. III-4.2 shows that $X_p/R_1 = \cos^2\beta(0)$. Hence

$$p_1 = -\cos^2\beta(0) \tan\beta(u) + u \qquad \text{(III-4.2)}$$

By making the substitution

$$(1 + \tan^2\beta(0)) = (\cos\beta(0))^{-2}$$

in Eq. III-2.4, we obtain

$$p_1(u) = -\left[\sin\beta(0)\cos\beta(0) + u + u^2\tan\beta(0) + u^3\tan^2\beta(0) + \ldots\right] - u$$

or

$$p_1(u) = -\left[\sin\beta(0)\cos\beta(0) + u^2\tan\beta(0) + u^3\tan^2\beta(0) + \ldots\right] \qquad \text{(III-4.3)}$$

For the circular cylinder, the terms are the same up to the u^3 term. The series is:

$$p_1(u) = -\left[\sin\beta(0)\cos\beta(0) + u^2\tan\beta(0) + u^3(\tan^2\beta(0) + \tfrac{1}{3}) + \ldots\right] \qquad \text{(III-4.4)}$$

5. Approximate Asymmetric Point-to-Point Geometries

It has now been shown that minimum Z-aberration is obtained

for the off-normal focus when it lies on the circle of least aberration. If the final shape is a cylinder of radius $R_2 = R_1$, however, the Y-aberration is equal to $(R_1 - X_p)\ \frac{b}{R_1}$, so that in this case there would be little advantage in going from F_1 to P_1 to improve the resolution. One way to reduce the Y aberration in order to obtain approximate asymmetric point-to-point focusing is to wrap the crystal on a cone whose axis is the line between the two focal points, P_1 and F_2. Another way is to make the final shape an elliptical cylinder whose two focal axes are the f-axis and the p-axis, or to approximate a part of the elliptical cylinder with a circular cylinder whose radius, R_2, is the geometric mean of R_1 and X_p. However all of these solutions introduce complicated small aberrations in both the Y and Z directions in the "point" focus, F_2, as well as in the conjugate focus, P_1 and will not be considered in further detail.

6. Approximate Symmetric Point-to-Point Geometry

We are not restricted to have one focus at Z = 0, however. If we place one focus at P_1 and the other at the other intersection, P_2, of the p-axis with the circle of least aberration, then we may eliminate Y aberrations entirely by letting $R_2 = X_p$ (cf. Fig. III-4.2 and Fig. III-6.1). In this case, we must make $\beta(0) = \frac{\pi}{2} - \theta$, where θ is the Bragg angle for the x-rays used. This also gives $\alpha(0) = 0$. The result is a symmetrical line-to-line focusing geometry, where the line foci have minimum average length for a given crystal width, a. This solution might thus be considered an approximate point-to-point focusing geometry, with Z-aberrations of order u^2 and higher.

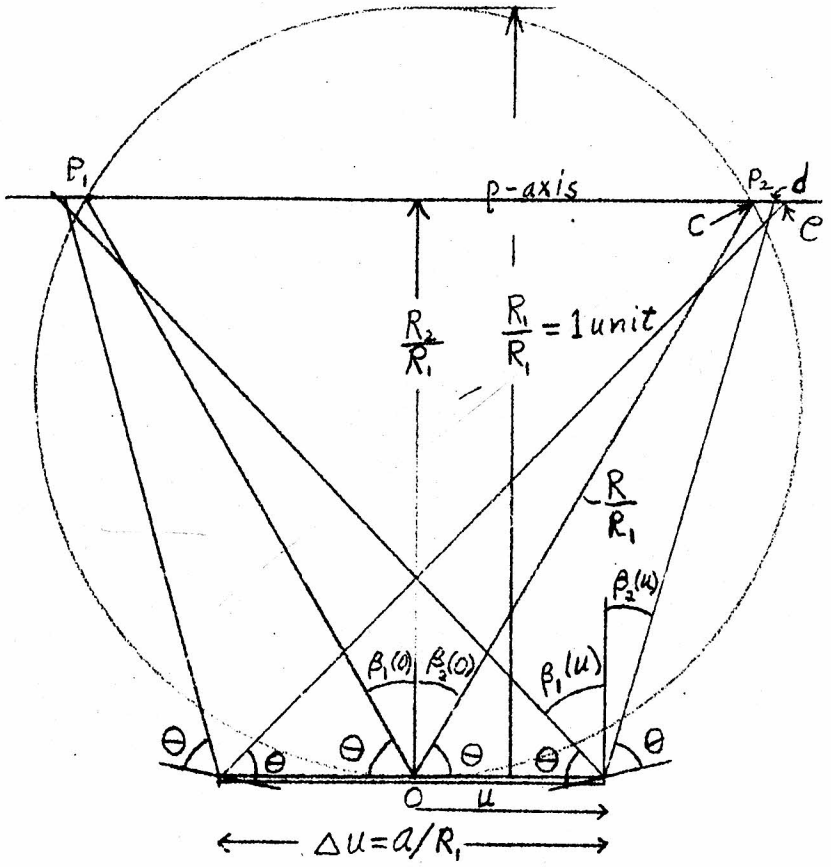

Fig. III-6.1 The monochromatic approximate point-to-point focusing geometry in dimensionless units.

θ = Bragg angle for the chosen wave-length.
$R/R_1 = \sin\theta$.
$R_2/R_1 = \sin^2\theta$.

p_1, p_2, and u are dimensionless metrics parallel to the crystal surface. c, d, and e are intersections of central and extreme rays with the p-axis.

Since the geometry is symmetrical, $\beta_1(u) = \beta_2(-u)$ (Fig. III-6.1). Other properties of the geometry are:

$$R_2 = R_1 \cos^2 \beta(0) = R_1 \sin^2\theta = R \sin \theta \qquad \text{III-6.1)}$$

where R is the length of the converging or diverging beam, just as in the perfect monochromatic point-to-point focusing geometry (cf. Eq. I-1.2).

Let $c = p_2(0)$, $d = p_2(-\frac{\Delta u}{2})$, and $e = p_2(\frac{\Delta u}{2})$, where $\Delta u = a/R_1$ (Fig. III-6.1). Then the Z-aberration will be given by the longest of the three line segments $\overline{cd}$, $\overline{ce}$, and $\overline{de}$. For an originally circular cylindrical lamina, Eq. III-4.4 gives

$$\overline{cd} \approx u^2 \tan\beta(0) = (\Delta u/2)^2 \cot \theta \approx \overline{ce} \qquad \text{(III-6.2)}$$

and

$$\overline{de} \approx (\Delta u)^3(\cot^2 \theta + 1/3) \qquad \text{(III-6.3)}$$

Thus, unless θ is nearly 90° and Δu is very large, the Z-aberration will be approximately equal to $(\Delta u/2)^2 \cot \theta$. To second order of approximation, the cosh curve would give the same aberration.

It should be noted that the Z-aberration at the focal circle is larger than the aberration along a line through the focal circle at p, and normal to the line $\overline{op}$, by a factor of $\csc \theta$. For purposes of calculation, however, it is usually easier to deal with Z-aberration than with the true minimum aberration.

7. Applications in X-Ray Spectrographs

Thus far, we have considered only monochromatic radiation and have assumed that the band of wave-lengths reflected at one angle, θ, was of negligible width. These calculations may be applied to find the resolution of x-ray spectrographs that might be constructed using the principle of double bending with developable surfaces in order to focus a large solid angle of rays from a small source more accurately than with a singly bent crystal.

The resolution of the perfect monochromatic focusing crystal discussed first is actually limited by the range of wave-lengths that may be reflected at any one angle. For nearly perfect crystals, such as quartz, this range would only be a few parts in 10^5 of the wave-length, for wave-lengths of the order of one Angstrom. However, for wave-lengths reflected toward points other than the normal focus, F_2, the resolution would rapidly diminish as the deviation from F_2 increases until the u^2 term (cf. Eq. III-2.4 and Eq. III-3.1), in the aberration thus produced, would become important, at which point the circular cylinder approximation would be nearly as good as the exact solution. It would be advantageous to use the cosh cylinder rather than the circular approximation for spectroscopy only in cases where it is desirable to resolve spectral structure over very small angular ranges, while using a large solid angle of crystal. Hence, the use of the cosh cylinder might be practical in the extremely high energy range with transmission focusing since, in that case, θ is always

very nearly 90 degrees. Use of the exact geometry might also be worth while in instruments designed to scan surfaces for fluorescent radiation, where one is always looking for the same wave-length, and it is desirable to have high resolution and to intercept a large solid angle of radiation.

However, a lamina of circular cylindrical shape is much easier to make, and has nearly the same resolution except at the normal focus. If such a lamina were mounted so that R_2 could be varied, a single crystal of this form could be adjusted to focus a wide range of wave-lengths. It would still allow the use of a larger solid angle than an ordinary singly bent crystal does, for the same resolving power, but the necessity of varying the second curvature would make it impractical except in cases where the source of radiation to be examined is very weak.

IV GEOMETRY FOR STRICT POINT-TO-POINT FOCUSING OF A SMALL FINITE BAND OF WAVE-LENGTHS

There are certain advantages to be gained by slightly relaxing the requirement of strict monochromaticity in order to obtain more perfect imaging of a point in the x-ray source as a point in the focused image formed by the reflecting crystal.

Although it is not possible to obtain point-to-point focusing of strictly monochromatic x-rays with a crystal lamina in the form of a developable surface, it is possible to obtain exact point-to-point focusing with such a lamina using a very narrow band of wave-lengths.

Since the reflection from the Bragg planes is essentially specular, the angle between the planes and the crystal surface as a function of u should be such that their normals, N, bisect the angle P_1 u P_2 between the two foci (Fig. IV-1.1). Only the crystal geometry that is symmetrical between the foci will be considered, since this geometry requires the minimum width of wave-length band for a given set of Bragg planes and a given width, a, of crystal.

The function $\alpha(u)$ for perfect point-to-point focusing may be found by noticing that in Fig. IV-1.1,

$$\phi = \arctan\left(\frac{u + \sin\theta(0)\cos\theta(0)}{\sin^2\theta(0)}\right) + \alpha = \arctan\left(\frac{-u + \sin\theta(0)\cos\theta(0)}{\sin^2\theta(0)}\right) - \alpha$$

or

$$2\alpha(u) = \arctan\left(\cot\theta(0) - \frac{u}{\sin^2\theta(0)}\right) - \arctan\left(\cot\theta(0) + \frac{u}{\sin^2\theta(0)}\right)$$

This function may be expanded in a Maclaurin series:

$$\alpha(u) = u - \frac{u^3}{3\sin^2\theta(0)} + \text{order } u^5 \qquad \text{(IV-1.1)}$$

Obviously there exists a function X(Z) such that a lamina cut to a cylinder of that shape from an unstressed crystal would have the above Bragg plane orientation, $\alpha(u)$. However, we have not obtained a closed expression for X(Z).

For practical purposes we only need to know how much aberration

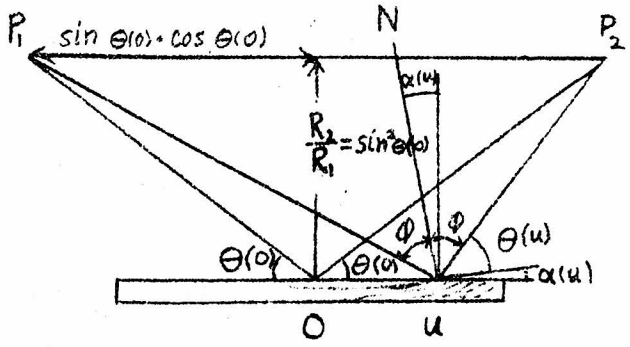

Fig. IV-1.1 The exact point-to-point focusing geometry for approximately monochromatic radiation, in dimensionless units.

N = normal to Bragg planes.
Ø = complement of the Bragg angle.

p_1 and p_2 are exact point foci.

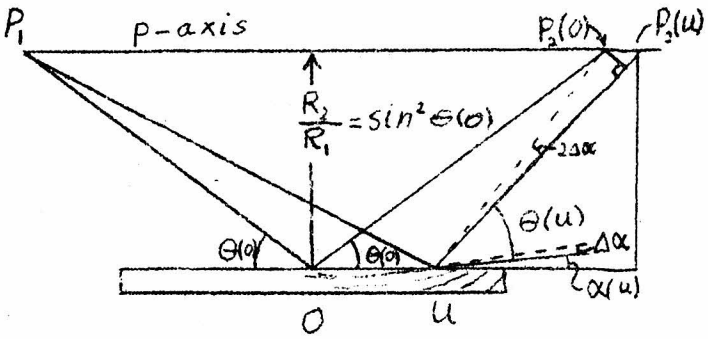

Fig. IV-1.2 Aberrations introduced by using an inexact function, $\alpha(u)$, with a point source, $p_1 \cdot \Delta\alpha$ = difference between the $\alpha(u)$ for exact focusing and the $\alpha(u)$ actually obtained with the crystal. $p_2(u)$ is the point where a beam reflected from a point, u, on the crystal recrosses the p-axis.

is obtained if we approximate the exact cylinder X(Z) with a circular cylinder. Suppose we assume the source, P_1, (Fig. IV-1.2) is a mathematical point of radiation of all wave-lengths in a broad band near $\lambda = 2d \sin\theta(0)$. If we make the original cylinder circular, and of radius R_1, and make the final form a circular cylinder of radius $R_2 = R_1 \sin^2\theta(0)$, then $\alpha(u) = u$ and $R = R_1 \sin\theta(0)$.

Let $\Delta\alpha$ be the amount by which α for a circular cylinder differs from α for a perfect focusing cylinder. Then, since $\alpha(u) = u$ for a circular cylinder, it may be seen from Fig. IV-1.2 that, to first order in $\Delta\alpha$,

$$p(u) - p(0) = \frac{2(\Delta\alpha)\cdot(R_2/R_1)}{\sin^2(\alpha(u)+\theta(u))}$$

$$= \frac{2\,\Delta\alpha \sin^2\theta(0)}{(\sin\theta(u)\cos u + \cos\theta(u)\sin u)^2} \approx \frac{2\,\Delta\alpha}{(1 + u\cot\theta(0))^2}$$

$$\approx 2\Delta\alpha(1 - 2u\cot\theta(0))$$

Using Eq. IV-1.1 for the perfect $\alpha(u)$, we get

$$\Delta\alpha = u - \left(u - \frac{u^3}{3\sin^2\theta(0)} + \text{order } u^5\right) \approx \frac{u^3}{3\sin^2\theta(0)}$$

so

$$p(u) - p(0) = \frac{2u^3}{3\sin^2\theta(0)} - \frac{4}{3}\frac{u^4}{\sin^3\theta(0)}\cos\theta(0) + \text{order } u^5 \qquad \text{(IV-1.2)}$$

In practical cases for use in low angle diffraction apparatus, we shall

see that this is too small an aberration to warrant correction (Part VI-3).

It should be noted that θ is not a constant, as it was in Part III, since we are now letting it equal the angle of incidence and of reflection from the Bragg planes, and requiring that reflection of x-rays of some wave-length originating at a point p_1 should take place at each point on the crystal, rather than that each point reflect a particular wave-length from an arbitrary point on the p-axis.

Let us now calculate $\theta(u)$ for the point-to-point geometries. We may see in Fig. IV-1.1 that:

$$\theta(u) - \alpha(u) = \arctan\left(\frac{\sin^2 \theta(0)}{\sin\theta(0)\cos\theta(0) + u}\right)$$

The Maclaurin series expansion of this function is:

$$\theta(u) - \alpha(u) = \theta(0) - \alpha(0) - u + u^2 \cot\theta(0) + \text{order } u^3$$

For any reasonable cylinder for this geometry, $\alpha(u) = u + \text{order } u^3$, (cf. Eq. IV-1.1). Hence

$$\theta(u) - \theta(0) = u^2 \cot\theta(0) + \text{order } u^3 \qquad \text{(IV-1.3)}$$

We may now use this equation to find how the wave-length reflected from the crystal depends upon its point of reflection, $u = z/R_1$. Differentiating Bragg's law, we obtain:

$$\Delta\lambda = 2d \cos\theta \, \Delta\theta$$

Hence, if the wave-length reflected at the center of the crystal is

$\lambda(0)$, we obtain

$$\lambda(u) = \lambda(0) + 2d \cos\theta \cdot u^2 \cot\theta + \cdots \approx \lambda(0)(1 + u^2\cot^2\theta) \qquad \text{(IV-1.4)}$$

V THE POINT FOCUSING MONOCHROMATOR FOR LOW ANGLE DIFFRACTION STUDIES

1. Requirements on the Instrument

X-ray diffraction and electron microscopy are the two methods available for study of particles and large molecular structures of dimensions up to two or three thousand Angstroms, at which dimensions ultraviolet microscopy and various indirect optical methods begin to be applicable.

Many materials, especially organic ones, such as viruses, protein molecules, and plastics, are destroyed or altered when placed in a vacuum, as is necessary for electron microscopy or for the use of x-rays longer than about five Angstroms, yet they have important structural details in the region above fifty or a hundred Angstroms and below the range of ultraviolet microscopy. Consequently, in order to study such materials, diffraction of x-rays, with wave-lengths just short enough to travel reasonable distances through air, helium, or water vapor atmospheres is employed. Since the resulting diffraction patterns subtend angles of less than one or two degrees, and down to the order of a few minutes of arc, the x-ray beam must be extremely well collimated, and at the same time it must be almost completely monochromatic to within about one percent of its wave-length.

One method of obtaining such a beam is to collimate it through a set of pinholes or slits, and to monochromatize it by using characteristic x-ray line radiation filtered through metal foils that absorb most of the unwanted wave-lengths. However, much better monochromatization may be obtained by using crystal reflection. Likewise, in cases where the angular resolution must be of the order of only a few thousandths of a radian, and where point focusing has advantages over line focusing, the use of a doubly curved crystal allows more total x-ray flux to pass through the x-ray focal spot than is allowed by a pinhole system of equal resolution. This is only true, however, if very perfect crystals, such as quartz, are used, because the angular resolution of the less perfect crystals is usually quite poor. Very accurate point focusing with quartz crystals was first achieved by Shenfil, Danielson, and DuMond (11), by using two singly bent cylinders of quartz in series, so oriented that the line focus of x-rays from the first crystal was focused toward a point by the second. The loss of intensity in two successive reflections, however, made exposure times so long that the apparatus could not be used to advantage on many perishable biological materials. It was this problem that prompted the invention of the developable surface bending principle and its first application.

2. Choice of Geometry

If an x-ray tube with a sufficiently long and fairly intense line focus were available, one could probably obtain the most x-ray

flux through the point focus of a doubly curved crystal monochromator by choosing the exact line-to-point geometry, described in Part III-2, and by relying on the spectral resolution of one of the characteristic x-ray lines by the crystal to make the focus a "point" in the Z direction.

However, from a practical standpoint, the point-to-point geometry seems a better choice for several reasons. Since, in this geometry, the point focus is an image of the source, the resolution of such an instrument may be controlled by varying the size of the source, either by adjusting the size of the focus of the electron beam incident on the target of the x-ray tube, or by putting various sizes of apertures in front of the focal spot of the tube at one focal plane of the crystal. Furthermore, fine point-focusing x-ray tubes can be run at a higher specific loading than line-focus tubes because the heat from a fine point focus may be dissipated faster than from a line focus. The central part of the converging beam may therefore be brighter with the point-to-point geometry than with the line-to-point geometry. Finally, although the useful solid angle is limited by the width of the spectral line in the point-to-point geometry, as will be explained in Part VI-1, the size of good crystals of quartz that are readily obtainable is not sufficient to take advantage of the unlimited useful size of crystal in the line-to-point geometry.

The useful crystal size limitation in the point-to-point geometry also makes the aberration introduced by using the circular cylindrical approximation for the unstressed lamina entirely negligible

for use in low angle diffraction.

Hence, for the single crystal point focusing monochromator already constructed, and for another now under construction, the circular cylinder approximation to exact point-to-point geometry was chosen.

3. Aberrations from Crystal Thickness

In all the preceding calculations, the crystal lamina was assumed to be so thin that its thickness could be neglected in calculating aberrations. The resolution often required for low angle diffraction studies is so high, however, that the possibility of the importance of this factor should not be overlooked. It will now be shown that for the point-to-point geometry with two real foci, the crystal thickness contributes a negligible aberration.

Let $\alpha(u)$ be the angle at which the Bragg planes intersect the midsurface of the crystal and let $\alpha(\xi, u)$ be the angle between the crystal planes and the surface at some distance $\xi = x/R_1$ from that surface (Fig. V-3.1). From Fig. V-3.2, we can see that $\alpha(\xi, u) = \alpha(u)$ before the crystal is flattened. Afterwards, $\alpha(u)$ is unchanged, but if the thickness of the crystal is unchanged, we get

$$\alpha(\xi, u) \approx \tan^{-1}\left(\frac{\tan \alpha(u)}{1-\xi}\right) \approx \tan^{-1}\left(\alpha(u) + \frac{\alpha(u)}{3}\right)(1+\xi)$$

$$\approx \tan^{-1}\left(\alpha(u) + \xi\alpha(u) + \frac{\alpha^3(u)}{3}\right)$$

or

$$\alpha(\xi, u) \approx \alpha(u)(1+\xi) \qquad \text{(V-3.1)}$$

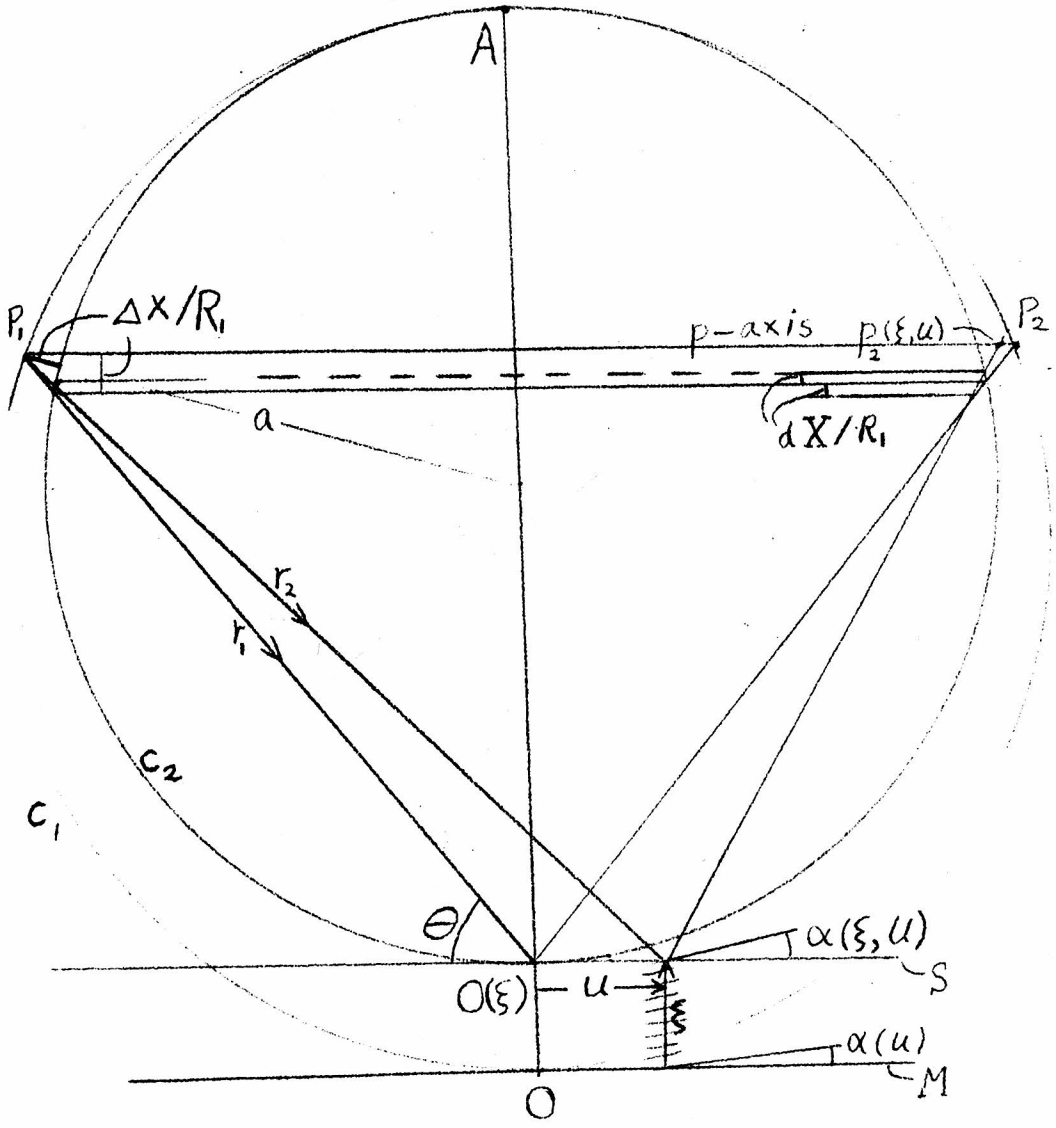

Fig. V-3.1 The aberration introduced by crystal thickness in exact point-to-point focusing geometry. u, p_1, p_2, and ξ are dimensionless metrics. M is the mid-surface of the crystal lamina. S is a surface parallel to M at a distance ξ from M. O = center of mid-surface of the crystal. O(ξ) = center of S. $\alpha(u)$ = angle of intersection of Bragg planes with M at u. $\alpha(\xi, u)$ = angle of intersection of Bragg planes with S at a. r_1 and r_2 are rays. c_1 = focal circle for M. c_2 = focal circle for S. a = radial line through c_1 at the position of the source, p_1.

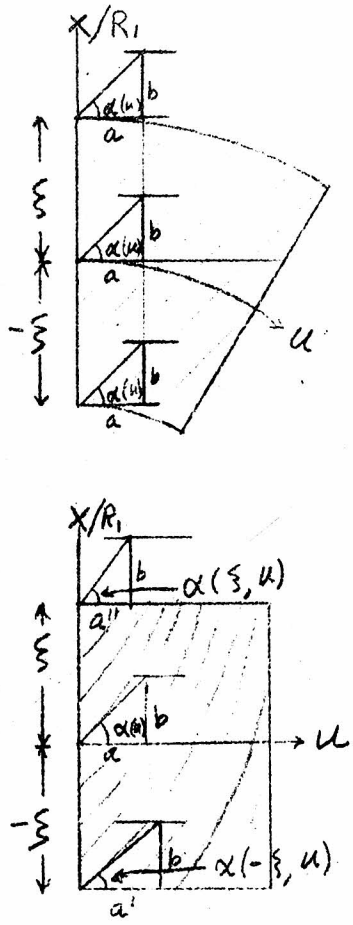

Fig. V-3.2 The effect, on α, of flattening a lamina of finite thickness. Strains change elements of length, such as a' and a'', parallel to the surfaces, except on the midsurface, M, but not those, such as b, normal to the surfaces.

to first order in $\S$ and third order in $\alpha(u)$.

This means, essentially, that for every layer, $x/R_1 = \S$, of the crystal lamina, the geometry is similar, but the scale is proportional to the distance $\overline{AO(\S)}$, where $\overline{AO} = R_1$. Now, if we draw two focal circles, (Fig. V-3.1; cf. Fig. I-1.1) through the midsurface at O and through the point $O(\S)$, they will both pass through the point A. If we now draw the paths of the rays reflected at the points $\S$, u, and at $O(\S)$ starting from a point p_1 on the focal circle that passes through the origin, O, we may see that

$$p_2(u, \S) - p_2(0) \approx ((2u/\sin^2\theta(0))\cdot(\Delta X/R_1)$$

where ΔX is the X distance between p_1 and the intersections of the rays with the smaller focal circle. The intersections are not all at exactly the same point, but the difference is of order u times ΔX and may be neglected. It may also be observed that the distance between the two circles at p_1 and p_2 is approximately equal to ΔX and to $(\S/2)(1+\cos 2\theta)$. Hence,

$$p_2(u, \S) - p_2(0) \approx 2u\S\left(\frac{1+\cos 2\theta}{2\sin^2\theta}\right) = 2u\S\cot^2\theta \qquad (V\text{-}3.2)$$

If the calculations had been done using the circular cylinder approximation, the additional aberrations independent of $\S$ would have made the geometry more complicated, but the result would clearly have been the same to the order of approximation obtained in Eq. V-3.2.

Since the thickness of quartz is limited, by its strength, to be less than about 10^{-3} R_2 and since u is usually less than 0.1, the

aberration introduced by thickness is usually negligible in practical applications.

VI INTENSITY OF BEAM REFLECTED FROM BENT CRYSTALS

1. Effect of Crystal Width

Since the wave-length band to be focused for low angle diffraction studies is supposed to be very narrow, the way to obtain high x-ray beam intensity is to choose a wave-length band near the spectral center of one of the characteristic x-ray lines of the source. Then, if the x-ray tube is run at a voltage several times the excitation potential for the spectral series of which the chosen line is a member, the contribution of the characteristic line radiation to the beam will outweigh that of the continuum by a very large factor. Hence, only the contribution of the characteristic radiation from one spectral line need be considered in calculating the intensity of the reflected beam.

It was shown in Part IV that the angles of incidence and of reflection, $\theta(u)$, for rays striking the crystal at a distance $u = z/R_1$ from the center of the crystal will increase as u increases. Hence, the center of the crystal will reflect a narrow band of wave-lengths $\lambda(0) \approx 2d \sin \theta(0)$, where d is the distance between Bragg planes. Farther out, longer wave-lengths, $\lambda(u) \approx 2d \sin \theta(u)$, will be reflected. This is illustrated in Fig. VI-1.1. We have already shown that the resulting dependence of λ on u is

$$\lambda(u) = \lambda(0)(1 + u^2 \cot^2\theta(0)) \qquad \text{(IV-1.4)}$$

It has been shown by Hoyt (12) that the intensity of radiation within a spectral line is well represented by the formula

$$J(\lambda - \lambda_o) = \frac{C}{1 + \left(\frac{\lambda - \lambda_o}{w}\right)^2} \qquad \text{(VI-1.1)}$$

where λ_o is the wave-length at the peak of the line, w is the half-width of the line at half-maximum intensity, and C is a proportionality factor (Fig. VI-1.1). The total intensity associated with the line, emitted in unit solid angle by the source, is

$$I_t = \int_o^\infty J(\lambda - \lambda_o)\, d\lambda = w \int_{-\infty}^{\infty} \frac{C}{1+x^2}\, dx = \pi C w$$

Hence,

$$C = I_t / \pi w$$

Suppose each point, u, on the crystal will reflect a fraction $R(\lambda, u)$ of x-rays of wave-length λ from the point source, and suppose we define a quantity, B, as

$$B \equiv \int_o^\infty R(\lambda, u)\, d\lambda \qquad \text{(VI-1.2)}$$

Let us further assume that contribution of $R(\lambda, u)$ to the integral is negligible except in a range of wave-lengths much narrower than the width, 2w, of the spectral line. The latter assumption is valid for very perfect crystals such as quartz, for most of the Bragg planes, with x-rays about as hard as copper $K\alpha_1$ radiation, as will be shown in the Part VI-3.

Then the fraction of the total incident flux, associated with

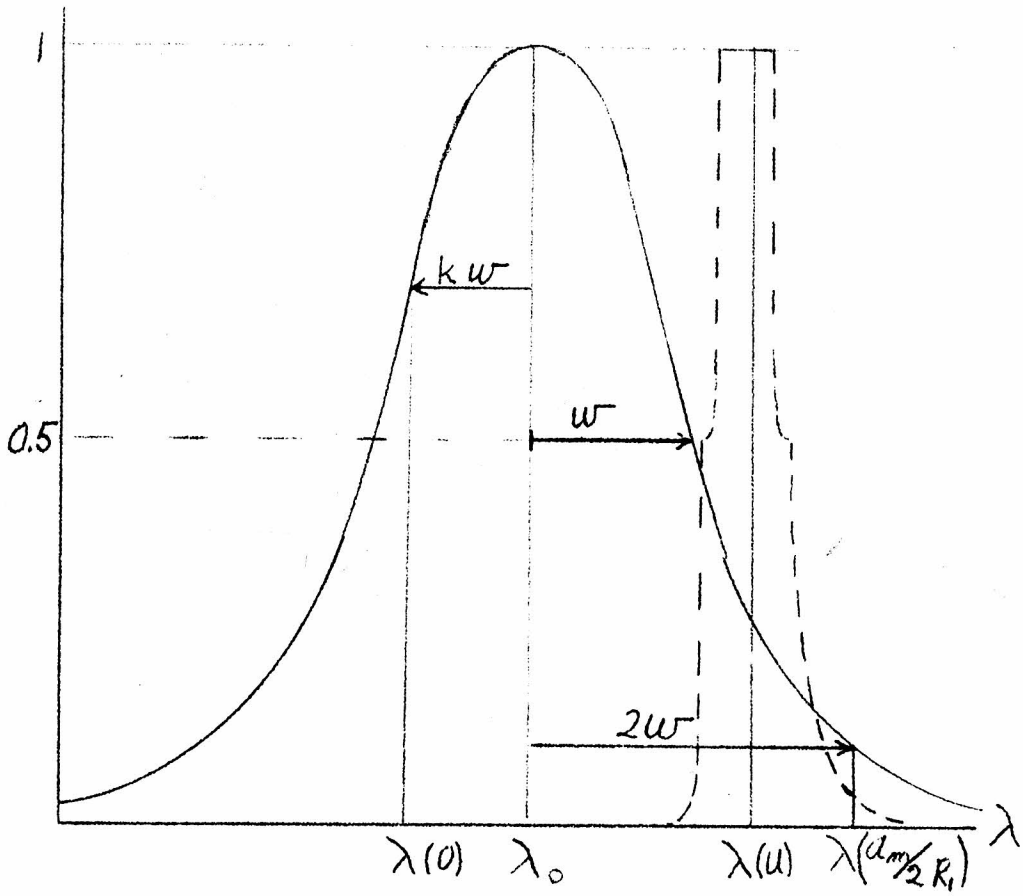

Fig. VI-1.1 Solid curve: $I(\lambda)$, the intensity in an x-ray spectral line as a function of λ, the wave-length, in units such that the center of the line, λ_0, has unit intensity. w = half-width of spectral line at half-maximum intensity.

Dotted curve: $R(\lambda, u)$, the fraction of the radiation of wave-length λ which will be reflected by the crystal if the angle of incidence is $\theta(u)$. (See Fig. IV-1.1).

the spectral line, that is reflected at any point on the crystal is

$$\frac{I(u)}{I_t} = B \cdot \frac{1}{\pi w} \cdot \frac{1}{1+\left(\frac{\lambda(u)-\lambda_o}{w}\right)^2} \qquad \text{(VI-1.3)}$$

The fraction of the total flux, emitted per unit solid angle by the source, that is reflected by the crystal will be

$$\frac{I}{I_t} = \int \frac{I(u)}{I_t}\, d\Omega \qquad \text{(VI-1.4)}$$

where $d\Omega$ is the solid angle subtended by an element of surface toward the source.

$$d\Omega = (b/R_1 \sin\theta)\cdot(dz/R_1 \sin\theta)\cdot \sin\theta$$

in the region near the center of the crystal. If we use $u = z/R_1$ and let $\eta = b/R_1 \sin\theta$, we obtain

$$I/I_t = \eta \frac{B}{\pi w} \int_{-a/2R_1}^{a/2R_1} \left[1 + (\lambda(u)-\lambda_o)^2\right]^{-1} du$$

$$= \eta \frac{B}{\pi w} \int_{-\Delta u/2}^{\Delta u/2} \left\{1 + \left[\lambda(0)(1+u^2\cot^2\theta(0)) - \lambda_o\right]^2\right\}^{-1} du$$

or

$$I/I_t = \eta \frac{B}{\pi w} \int_{-\Delta u/2}^{\Delta u/2} \left[1 + (hu^2 - k)^2\right]^{-1} du \qquad \text{(VI-1.5)}$$

where

$$h \equiv \frac{\lambda(0)}{w} \cot^2\theta(0) \qquad \text{and} \qquad k \equiv \frac{1}{w}\left(\lambda_o - \lambda(0)\right) \tag{VI-1.6}$$

If the crystal were infinitely wide, we would have $\Delta u = \infty$, so that the maximum obtainable value of I/I_t is

$$I_m/I_t = \frac{\eta B}{\pi w}\frac{1}{h^2}\int_{-\infty}^{\infty}\left[u^4 - 2\frac{k}{h}u^2 + (k^2+1)\right]^{-1} du$$

This integral may be solved by the method of residues with complex variables, and gives

$$I_m/I_t = \frac{\eta B}{\pi w}\cdot\frac{1}{h^2}\cdot\left[\frac{\pi}{2}\left(\frac{h^2}{k^2+1}\right)^{3/4}\cdot\frac{1}{\sin\left(\frac{1}{2}\tan^{-1}\frac{1}{k}\right)}\right]$$

which may be more conveniently written

$$I_m/I_t = \tfrac{1}{2}\,\eta\cdot\frac{B}{w}\cdot h^{-\frac{1}{2}}\cdot f(k) \tag{VI-1.7}$$

where

$$f(k) \equiv \left[(k^2+1)^{3/4}\sin\left(\tfrac{1}{2}\tan^{-1}\frac{1}{k}\right)\right]^{-1} \tag{VI-1.8}$$

Fig. VI-1.2 is a plot of the function f(k). One may observe that its maximum is at $k \approx 0.8$, at which point $f(k) = 1.676$. The value of k for large values of f(k) is clearly not critical.

Thus, if we had a crystal of infinite width, we could obtain

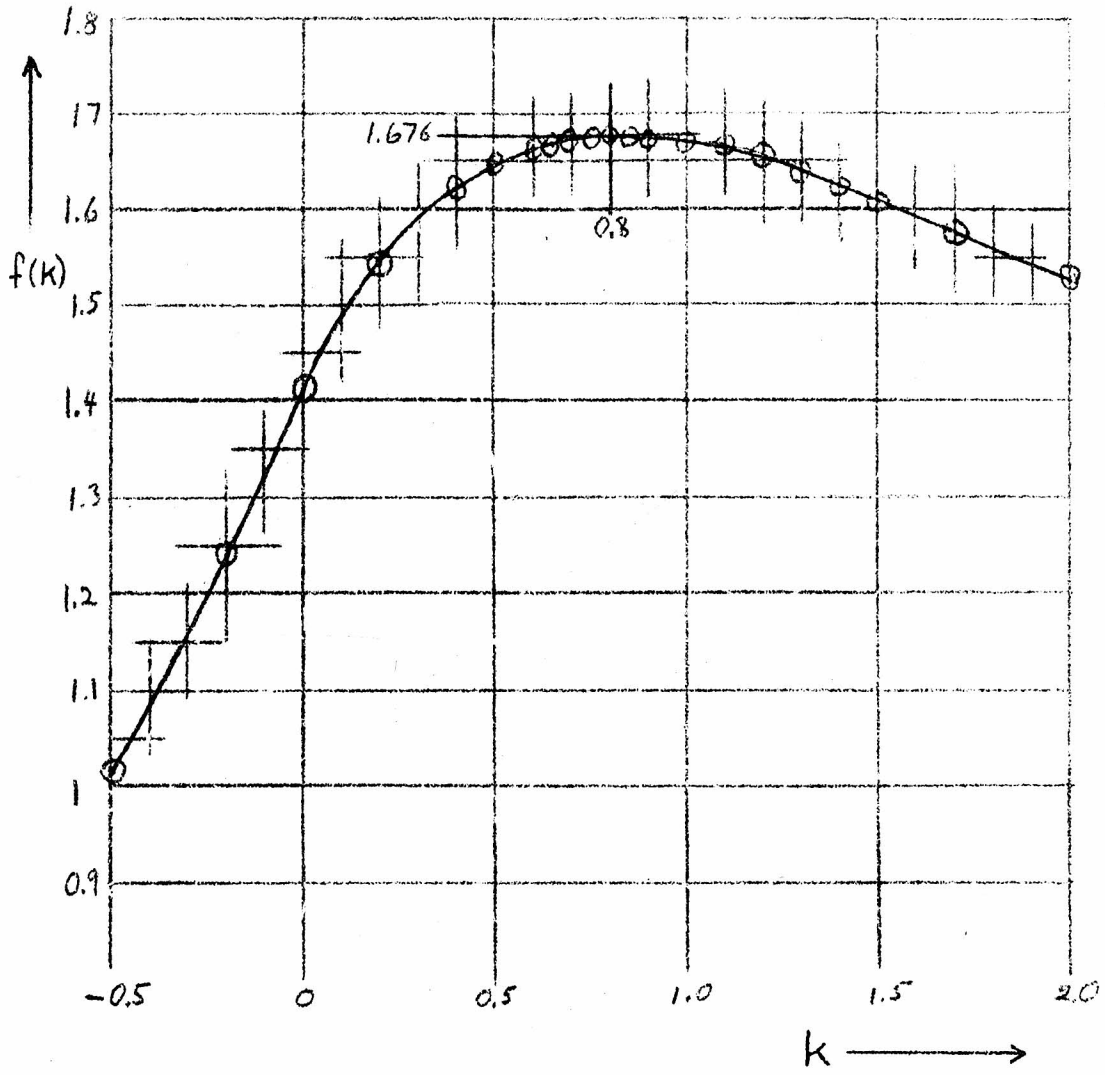

Fig. VI-1.2 The function $f(k) = (k^2 + 1)^{-3/4} \csc(\frac{1}{2} \cot^{-1} k)$. k is a measure of the difference between $\lambda(0)$ for the crystal, which depends on the orientation of the crystal and source, and λ_0, the wave-length of the center of the x-ray line. (See Fig. VI-1.1) The total flux reflected by the crystal is proportional to f(k). Notice that f(k) declines rapidly if k is too small, but slowly if it is too large.

an intensity

$$I_m/I_t = \frac{1.676}{2} \eta \frac{B}{w} h^{-\frac{1}{2}} \qquad \text{(VI-1.9)}$$

There will be very little loss in intensity if the crystal terminates at a point where $\lambda(u) = \lambda_o + 2w$, since the integrated intensity beyond that point only amounts to the order of one percent of the total for an infinite crystal. Let us call the width of a crystal that terminates according to the above formula, a_m (Fig. VI-1.1). Then

$$\lambda(a_m/2R_1) - \lambda(0) = \lambda_o + 2w - (\lambda_o + kw)$$

$$= (2 + k)w$$

Hence, we obtain an intensity almost as large as I_m/I_t (Eq. VI-1.9) if

$$\lambda(a_m/2R_1) - \lambda(0) = 2.8\ w \qquad \text{(VI-1.10)}$$

and since

$$\lambda(u) - \lambda(0) \approx \lambda(0)\ u^2 \cot^2\theta(0) \qquad \text{(IV-1.4)}$$

we get

$$(a_m/2R_1)^2 \cot^2 \theta(0) \approx 2.8\ w/\lambda(0)$$

or

$$a_m/R_1 \approx 2(1.67 \tan \theta_o)\left(\sqrt{\frac{w}{\lambda_o}}\right) = 3.34\ h^{-\frac{1}{2}} \qquad \text{(VI-1.11)}$$

where θ_o is the Bragg angle for λ_o.

Another useful formula is the one for a crystal of width much less than a_m, so that the whole crystal may be oriented to focus wave-lengths very near the peak of the spectral line. In that case,

$$I/I_t \approx \frac{B}{\pi w} \int d\Omega = \frac{B\eta}{\pi w} \cdot \Delta u = \frac{B}{\pi w} \cdot \frac{ab}{R_1^2 \sin\theta} \qquad \text{(VI-1.12)}$$

The fraction of all the x-radiation associated with a given characteristic x-ray line that is reflected in unit solid angle by a crystal will be called the reflection coefficient, ρ. Clearly

$$\rho = \frac{I}{I_t} \cdot \frac{R_1^2}{ab \sin\theta} = \frac{B}{\pi w \sin^2\theta} \qquad \text{(VI-1.13)}$$

The foregoing equations are valid for crystals of the perfect point-to-point focusing shape, and are somewhat inaccurate when the crystals used are as wide as a_m and are of the circular cylinder approximation form. Furthermore, we have assumed that source is an absolute point. The formulas become decreasingly accurate as the size of the source increases. The importance of these two factors should be tested when the formulae are used.

The criterion for the permissibility of neglecting the finite size of the source in the preceding equations is the following: The angle subtended in the XZ plane by the source, from the crystal center, must be somewhat less than the angular spreading of the characteristic x-ray line due to the spectral dispersion of the crystal.

Since the dispersion of the crystal is $\Delta\lambda/\lambda = \cot\theta\, \Delta\theta$, it

follows that the projection of the width of the focal spot on a line in the XZ plane, normal to the beam, should be less than $(Rw/\lambda)\tan\theta$. where w is the half width of the line at half maximum intensity, and R is the distance from the crystal to the source.

If we let the projected focal spot width be S, we may write the criterion thus:

$$S < (Rw/\lambda)\tan\theta \qquad \text{(VI-1.14)}$$

The source size may be fairly large in the Y direction without invalidating the equations or decreasing the monochromaticity of the beam. Hence, if it is desirable to sacrifice resolution along one axis, for higher intensity, a short line source in the Y direction might be used in place of a point.

2. Surface and Thickness Factors

The only undetermined factor in the preceding formulae for reflected intensity was B. This factor may be calculated by using Darwin's (3) or Ewald's (4) theories of x-ray reflection from perfect crystals if we assume that the bending does not disrupt the crystal structure enough over small regions to make their theories inapplicable. This assumption has been shown to be valid only if the bending is extremely slight (13), but the calculations will at least give some idea of the relative values of reflected intensity to expect from various sets of Bragg planes in any one type of crystal.

If we neglect the effect of absorption on the interference of x-rays striking the first surface of the crystal, Darwin and Ewald have shown that a particular wave-length will be totally reflected over a very narrow range of angles of incidence, provided that the Bragg planes are parallel to the surface, which is the case near the center of the crystal in the point-to-point geometry. Conversely, it may be seen that since different wave-lengths tend to reflect at different angles, a very narrow band of wave-lengths will be totally reflected at any particular angle of incidence.

The results obtained by the approaches of Darwin and Ewald are the same in the range of angles of total reflection, but differ somewhat in the adjacent region where rapidly diminishing partial reflection occurs. Darwin's theory predicts that the contribution of the partially reflecting region will be one fourth of the total, while Ewald's predicts two fifths.

Since absorption is neglected, let us also neglect the regions of partial reflection. This will make calculations simpler and will also tend to counterbalance the error introduced by neglecting absorption. The results we obtain are only intended to give a rough estimate of the reflected beam intensity.

The two theories indicate that x-rays that are totally reflected do not penetrate the crystal, to a significant amount, to depths of more than a few thousand Bragg planes, or a few thousand Angstroms. The first calculations will only deal with the reflection effect in the Bragg planes adjacent to the first crystal surface. The contribution of such reflection will be called the surface factor. X-rays of

wave-lengths somewhat too long to be reflected at the surface may travel on into the crystal and be partially reflected from some depth inside. This will be called the thickness factor.

According to Darwin, the angular band of total reflection of one-wave-length at the surface is

$$\Delta\theta_\sigma = 2\delta FZ^{-1} \sec\theta_o \csc\theta_o \qquad \text{(VI-2.1)}$$

for radiation polarized parallel to the plane of reflection and

$$\Delta\theta_\pi = \Delta\theta_\sigma \cos 2\theta_o \qquad \text{(VI-2.2)}$$

In these equations, δ is the unit decrement of the index of refraction and is fairly accurately given by classical electrodynamical theory:

$$\delta = \lambda^2 \frac{n}{2\pi} \frac{e^2}{m_o c^2} \qquad \text{(VI-2.3)}$$

where n is number of electrons per unit volume in the crystal. The factor FZ^{-1} is the structure factor for the set of Bragg planes, divided by the number of electrons in the unit cell of the crystal lattice. There are extensive tables of values of F for common crystals. Wei (14) has made a very exhaustive study of values of F for various planes in quartz.

Bragg's law, $\lambda = 2d \sin\theta$ for first order reflection, is accurate enough to calculate the change in angle of the center of the angular band of total reflection with wave-length, even though it must be modified very slightly to give the exact angle of the center of the band, according to Darwin's or Ewald's theory.

Differentiating Bragg's law gives:

$$d\lambda/\lambda = \cot\theta \, d\theta \qquad \text{(VI-2.4)}$$

where θ may be any value near $\theta(0)$, and λ may be any value near $\lambda(0)$ or λ_o for our purposes. If the radiation from the source is completely unpolarized, then the effective angular range of total reflection will be

$$\Delta\theta = \frac{\Delta\theta_\pi + \Delta\theta_\sigma}{2} = \delta F Z^{-1} \sec\theta \csc\theta(1 + |\cos 2\theta|) \qquad \text{(VI-2.5)}$$

Hence, if the angle of incidence is fixed, a range of wave-lengths

$$\Delta\lambda = \lambda \cot\theta \, \Delta\theta = \lambda\delta F Z^{-1} \csc^2\theta(1 + |\cos 2\theta|) \qquad \text{(VI-2.6)}$$

will, in effect, be totally reflected. We are assuming that other wave-lengths will not be reflected at all from the region near the surface of the crystal.

Notice that if it were not for the thickness factor, the value of $R(\lambda, u)$ in the intensity formulae would be unity in the region of total reflection of π radiation, roughly one half out to the edge of the region of reflection of σ radiation, and almost zero elsewhere. Hence, the quantity B would be equal to the effective value of $\Delta\lambda$ calculated above. Let us divide B into two parts: B_s for the surface factor, and B_t for the thickness factor. Then

$$B = B_s + B_t = \lambda\delta F Z^{-1} \csc^2\theta(1 + |\cos 2\theta|) + B_t \qquad \text{(VI-2.7)}$$

Now let us find the thickness factor. If we refer back to

Eq. IV-1.1 and Eq. V-3.2, we will notice that the first term in the angle α, which Bragg planes make with the crystal surface in point-to-point geometry, is $\alpha = u = z/R_1$, regardless of the depth within the crystal lamina. This is most obvious very near the center of the crystal. Fig. VI-2.1 shows a beam incident near the center of the first crystal surface. The angle of incidence with the Bragg planes there is θ, and the value of x is t/2. If a certain quantum in the beam is not of the correct wave-length to be reflected when the angle of incidence is θ, it will travel on into the crystal, and in doing so will come upon other planes at angles $\theta + \alpha_r - \alpha_i$, but with essentially the same Bragg spacing as at the first surface. The angle α_i is the angle of the planes at the point of intersection of the incident beam with the first crystal surface, and α_r is the angle of the planes with respect to the surface at a point r within the crystal lamina. By passing to a depth $\Delta x = (t/2) - x_r$ in the lamina, such a quantum passes through a range of angles of incidence

$$\Delta\theta = \alpha_r - \alpha_i = \frac{1}{R_1}(z_r - z_i) \approx \frac{1}{R_1}\,\Delta x \cot\theta$$

The probability, $P_e(\Delta x)$, that it will emerge at z_e is equal to the product of the probability, P_r, that it will be reflected at r times the probability, P_t, that it will travel through a distance $\overline{z_i\ r\ z_e}$ (Fig. VI-2.1) through the crystal without being absorbed. If the linear absorption coefficient of the crystal is constant, and equal to u, then:

$$P_t = e^{-\mu \cdot 2\,\Delta x \csc\theta} \qquad \text{(VI-2.8)}$$

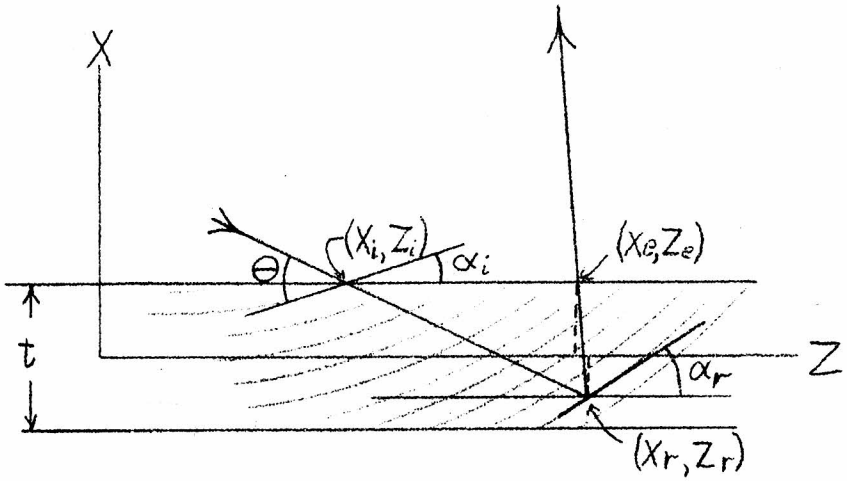

Fig. VI-2.1 A ray being reflected at a point (x_r, z_r) inside a crystal of thickness t. z_i, z_r, z_e are z-coordinates at points of incidence, reflection, and emergence. θ is the angle between the ray and any Bragg plane. θ depends primarily on z.

There is a small range of angles near the Bragg angle at which μ becomes very much less than its normal value. This fact may be explained by the use of Ewald's theory, as it is presented by Zachariasen (1) and pointed out by G. Borrman (16). However, this effect is not of major importance here, since the angular range of this anomalous transmission is about the same as the Darwin band width for total reflection, which is, in most cases, only a small fraction of the range of angles, $\Delta\Theta$, through which an internally reflected quantum will pass while it is inside the crystal. Hence, anomalous transmission will not be considered in these calculations.

Since the interference effects for internal reflection do not begin at the surface, the reflection properties inside might be expected to be more similar to those in transmission geometries than to those where reflection takes place near the surface of unbent crystals.

Solutions to Darwin's or Ewald's equations only indicate a band of total reflection if the Bragg planes are parallel to the surface of the crystal and if the beam enters at the Bragg angle. If the planes are normal to the surface, then, neglecting absorption, a certain fraction of the beam will be reflected by the planes and the rest will go on through in the transmitted direction. This fraction oscillates sinusoidally and rapidly between zero and one as the beam goes through a crystal, so that on the average, half the beam will go in the reflected direction after passing through a crystal of non-uniform thickness.

In the case of the bent crystal with internal reflection, therefore, let us make the assumption that once a ray gets to a depth where it is at the Bragg angle, it will be reflected back and forth in a layer a few thousand Bragg planes thick. Assume that it continues this action until it has traveled a distance that is short in comparison to its total path inside the crystal, and then is thrown off, because of the change in α with z, in either the reflected or transmitted direction, with equal average probability. If these assumptions are correct, then $P_r = 0.5$ so that

$$P_e(\Delta x) = 0.5\, e^{-\mu \cdot 2 \Delta x \csc \theta} \qquad \text{(VI-2.9)}$$

Hence, for a given point of incidence, u_o, on the first crystal surface, $R(\lambda, u_o)$ (Eq. VI-1.2) should equal unity in the band of total surface reflection, and in the region of wave-lengths too long for surface reflection it should be about equal to $P_e(\Delta x)$, where, from Eq. VI-2.4, we get

$$\Delta x = \Delta z \tan \theta = R_1 \theta \tan \theta = R_1 \frac{\Delta\lambda}{\lambda} \frac{\tan^2 \theta}{2}$$

Thus, we obtain

$$R(\lambda, u_o) = 0.5\, e^{-\mu R_1 \tan^2 \theta \csc \theta (\Delta\lambda/\lambda)} \qquad \text{(VI-2.10)}$$

in the region just on the long wave-length side of the region of total reflection for either the π or the σ component. This is illustrated, along with the R for total reflection, in Fig. VI-2.2.

The thickness factor, B_t, is thus given by

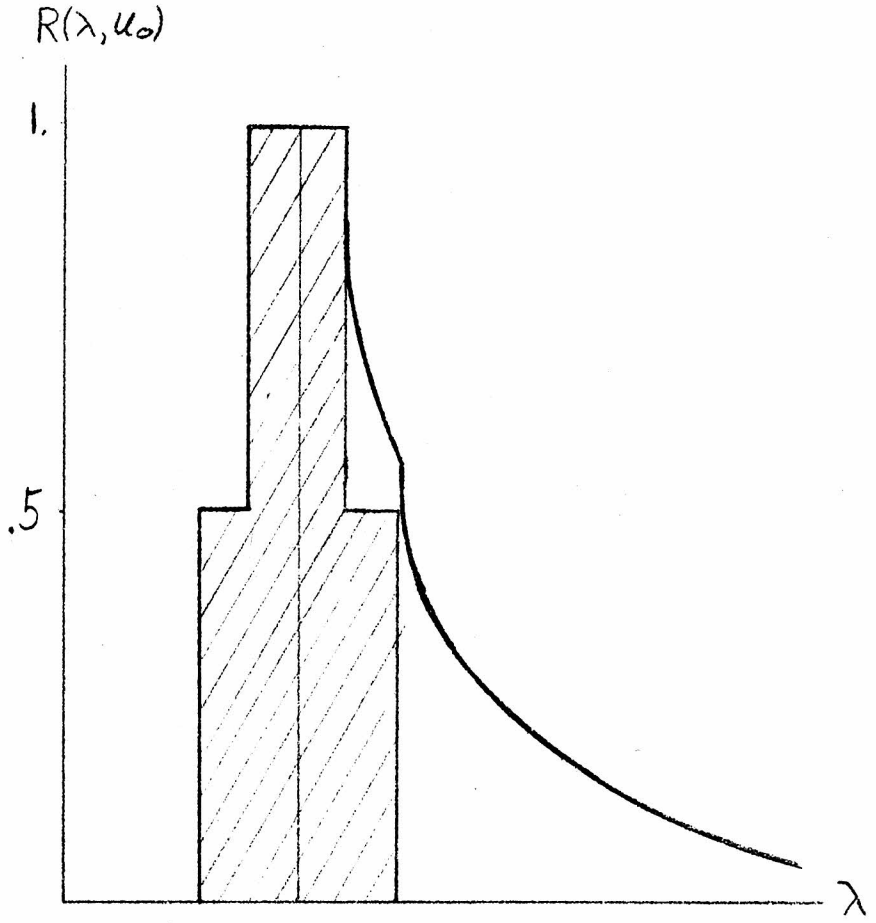

Fig. VI-2.2 $R(\lambda, u_o)$, the fraction of the radiation from a single ray, incident at u_o, that will be reflected from an ideally perfect curved crystal in point-to-point focusing geometry as a function of λ. The cross-hatched section is the contribution from near the first crystal surface; the blank section is the contribution from inside the crystal.

$$B_t = \int_0^{\Delta\lambda(t)} 0.5 \exp(-\mu R_1 \tan^2\theta \csc\theta \frac{\Delta\lambda}{\lambda}) \, d(\Delta\lambda) \qquad \text{(VI-2.11)}$$

If the quantity $(2\mu \csc\theta)(t)$ is greater than about two, we will make little error by taking the integral for B_t from zero to infinity, so that

$$B_t = \frac{0.5}{\mu R_1} \lambda \cot^2\theta \sin\theta \qquad \text{(VI-2.12)}$$

For this case, which is the usual one,

$$B = B_s + B_t = \lambda\delta FZ^{-1}\csc^2\theta(1 + |\cos 2\theta|) + \frac{\lambda}{2\mu R_1} \cot^2\theta \sin\theta \qquad \text{(VI-2.13)}$$

3. Sample Calculations

Let us now apply the formulae we have derived to some Bragg planes in quartz, using copper $K\alpha_1$ radiation. In order to find B_t, we must know the thickness, t, and radius of curvature, R_1, of the crystal. Since the limiting resolution due to irregularities in the crystal is roughly proportional to the distance, R, from the crystal to the focal spot, rather than to R_1, let us fix a value of $R = R_1 \sin\theta$ for comparing values of B_t. Let us choose R = 1 meter and $t = 2.5 \times 10^{-4}$ meters. A quartz crystal of that thickness falls just within the limit of safe curvature when the curvature is appropriate for the 011 planes, using copper $K\alpha_1$ radiation, and is thinner than necessary for the 052 and 023 planes.

First, notice that for t = .25 mm., $2\mu t \csc\theta = 4.1 \csc\theta$, which is much greater than two for any value of θ. Hence, Eq. VI-2.12 is valid, and we may use it to calculate B_t. With these choices, we may make a table of sample calculations (Table VI-3.1).

Comparison of S and $\Delta p_m \cdot R \sin^2\theta$ shows that for the 052 and 011 planes the aberration, $\Delta p_m \cdot R \sin^2\theta$, introduced by the circular cylinder approximation is larger than the maximum allowable source size, S, for applicability of equation VI-1.9 for I_m/I_t. Hence, to obtain maximum resolution and maximum total beam intensity with those two planes, one would have to use a more nearly exact curve than a circular cylinder. However, since aberration is proportional to a^3, the equations for I/I_t and ρ should be applicable to any of the planes for crystals that are only half as wide as a_m.

Table VI-3.1 Sample Calculations

λ_o = 1.5374 Å (15) w = 0.00029 Å (15)

δ = 8.1×10^{-6} (15) μ = 8.2×10^{3} per meter (15)

Z = 90 electrons per unit cell ($3 \cdot S_i O_2$)

Quantity	Equations or References	Values		
Bragg Plane		052	023	011
F	(14)	21.7	31.2	37.8
θ_o	(18)	71° 42'	34° 5'	13° 20'
B_s	Eq. VI-2.7	0.601×10^{-5} Å	1.66×10^{-5} Å	18.6×10^{-5} Å
B_t	Eq. VI-2.12	0.923×10^{-5} Å	6.35×10^{-5} Å	8.87×10^{-5} Å
$B = B_s + B_t$		1.524×10^{-5} Å	7.01×10^{-5} Å	27.47×10^{-5} Å
a_m	Eq. VI-1.11	0.147 M	0.055 M	0.047 M
I_m/I_t	Eq. VI-1.9	0.0019 b	0.0033 b	0.0111 b
I/I_t	Eq. VI-1.12	0.0159 ab	0.0432 ab	0.0678 ab
ρ	Eq. VI-1.13	0.0167	0.077	0.295
S	Eq. VI-1.14	0.56×10^{-3} M	0.127×10^{-3} M	0.045×10^{-3} M
$\Delta p_m \cdot R \sin^2\theta$	Eq. IV-1.2	2.13×10^{-3} M	0.111×10^{-3} M	0.068×10^{-3} M

The most important results in Table VI-3.1 are: a_m = maximum useful crystal width. I_m/I_t = maximum reflectivity. I/I_t = reflectivity of narrow crystals. ρ = reflection coefficient, or fraction of incident line radiation actually reflected, for narrow crystals. S = maximum source size. $\Delta p_m \cdot R \sin^2\theta$ = aberration from circular cylinder approximation.

The values for ρ indicate that with the 011 planes, one might expect 29.5 percent of the $K\alpha_1$ line to be reflected. However, the focal spot may only be about one twentieth of a millimeter across, with the dimensions chosen, if this high reflection coefficient is to be obtained. The apparent advantage of the 011 over the 023 planes vanishes for practical cases because it is practically impossible to figure cylinders with sufficient accuracy to obtain resolution as fine as one twentieth of a millimeter at a distance of one meter from the crystal.

Remembering that $w = 29 \times 10^{-5}$ Å for copper $K\alpha_1$ radiation we may see that Eq. VI-1.9 and Eq. VI-1.12, which were derived assuming the width of the important part of $R(\lambda, u)$ is much less than the spectral line width, are quite good for the 052 and 023 planes, although they would be somewhat inaccurate for the 011 planes. For slightly harder x-ray lines, the preceding assumption is not valid for thick crystals because μ becomes smaller so that the thickness factor, B_t, becomes larger. For much softer x-ray lines, δ becomes larger so that the surface factor, B_s, becomes larger and again the assumption becomes rather poor. However, for low angle diffraction work on biological materials in air or helium, wave-lengths near that of copper $K\alpha_1$ radiation are about the most convenient to use. Hence, the formulas derived are applicable in the region of wave-lengths which is of interest for our purpose.

VII DESIGN AND CONSTRUCTION OF A POINT FOCUSING MONOCHROMATOR

1. Choice of Crystal and Wave-Length

In making the first working model of a point focusing monochromator using the principles described in the preceding parts, quartz was chosen for the crystal because it has almost ideally perfect lattice structure and because it is sufficiently strong to be sawed, ground, polished, and elastically bent to appropriate radii. Furthermore, it has many sets of Bragg planes of different spacings with reasonably high structure factors, so that suitable planes may be found for a variety of different wave-lengths and Bragg angles.

Copper Kα radiation was chosen primarily because its wave-length is about the longest of the characteristic x-ray lines that will travel through a fairly long air path and through various organic and light metal films that are convenient to use for holding samples. Another advantage of using copper radiation is that an x-ray tube with a copper target may be run at a much higher specific power loading than is permissible with other target elements in that region of the periodic table.

In making the new point focusing monochromator, we were extremely cautious about bending the crystals. Since the stresses in the crystal are roughly proportional to t/R_2, the most compact geometry for a given crystal thickness is obtained when the Bragg angle, θ, is nearly 90 degrees. Hence, we chose the 052 Bragg planes, even though they are far from being the best reflectors of the chosen radiation. For the foregoing reason, and also for the purpose of making the background

from incoherent scattering negligible, we chose to make the scale of the instrument such that R is one meter, even though a smaller value of R would give a larger solid angle of x-ray beam with a crystal of the same area. The value of R_2 with these choices is 95 cm.

From cost considerations, and as this was a new experiment, we did not try to obtain the largest usable crystal size. The piece that was finally obtained was only 3.8 by 7.6 cm. The aberrations were minimized by choosing the short dimension as the width, a (Fig. II-1.1).

Before proceeding, it should be noted that we have tried bending the crystal laminae we obtained to much smaller radii, and found that it is possible to bend them to $R_2 = t \times 10^3$ without breaking them. Since t may be made equal to 0.25 mm. without extreme difficulty, it would even be possible to use the 011 planes with R = 1 meter if that were desirable. A new instrument is now being constructed using the 023 planes.

Of the various planes in quartz, the 011, 023, and the 052 planes are probably the best in their respective regions of Bragg spacings, according to the values of F given by Wei (14).

One other important possibility to note is that chromium $K\alpha$ radiation, although a little too soft for use in air, has two great advantages over copper $K\alpha$. It gives larger diffraction patterns with other dimensions the same, and it is also scattered more by sample materials, so that in cases where volume of sample material is at a premium, it might be very worth while to use chromium radiation. This

radiation will pass through helium at one atmosphere pressure with negligible loss. Chromium will not stand as much specific loading as will copper, but it is by far the best x-ray tube target material among the lighter elements.

2. The Mounting System

The first mounting used to hold the crystal in its proper final shape was a double frame of stainless steel, b and f, (Fig. VII-2.1), with the interfaces ground and lapped, by a method described by J.W.M. DuMond (18), to the appropriate cylindrical shape. A thin rubber gasket was placed between the concave part of the frame, b, and the crystal, c , and the two parts of the frame were bolted together at the four corners. We were unable to get a satisfactorily uniform curve for our purposes by this method. The crystal seemed to buckle and wrinkle around the edges when sufficient pressure was applied to curve it properly in the center. The best focus obtained with this mounting system was about two millimeters in diameter in its brightest region, and it had a great deal of irregular halo around the edges from disoriented areas on the crystal.

Far better results were obtained using a single stainless steel backing block, b (Fig. VII-2.2), which was lapped to the correct cylindrical shape, and against which the crystal, c, was held by atmospheric pressure.

A single hole of about one millimeter diameter was drilled through the center of the steel block before grinding and lapping,

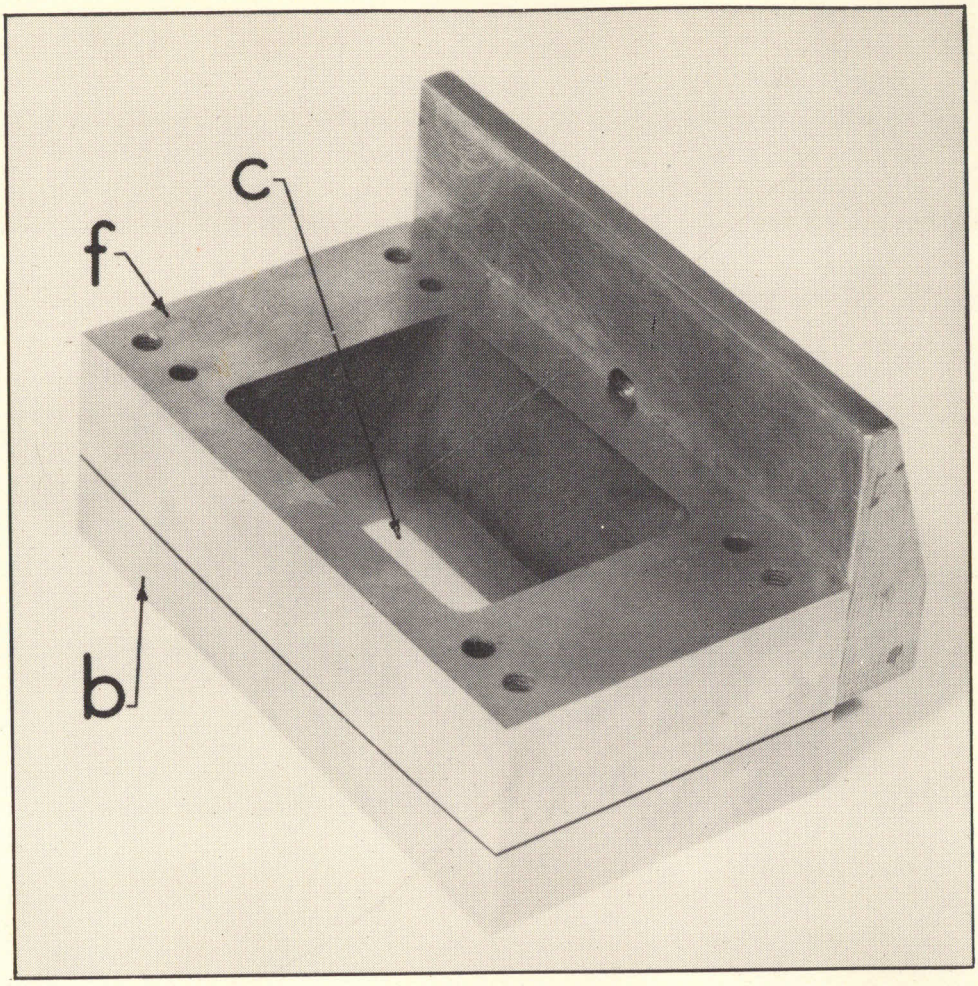

Fig. VII - 2.1. The double frame crystal mount.
c = crystal. b, f = double frame.

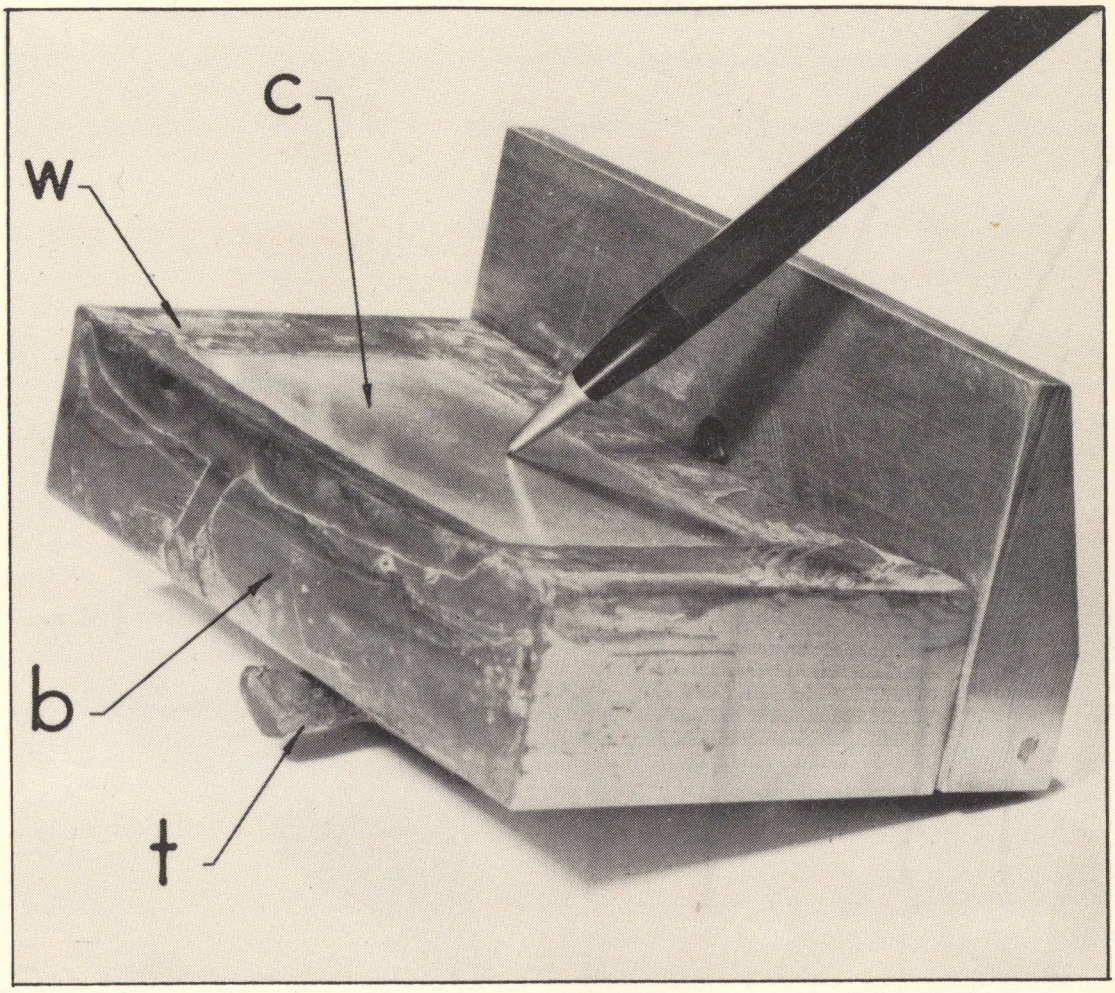

Fig. VII - 2.2. The vacuum crystal mount. c = crystal.
w = beeswax. b = stainless steel block.
t = exhaust tube.

through which the air could be evacuated from behind the crystal. (The hole may be seen faintly through the crystal at the tip of the lead pencil in Fig. VII-2.2.) A copper tube was attached to the back end of the hole with a brass fitting and beeswax. The pinched-off end of the tube, t, is seen protruding from below the steel block. A water aspirator was connected to this tube by means of a rubber hose to evacuate the air from between the crystal lamina and the steel block. After cleaning and removing the dust from the crystal and the steel backing block, the crystal was placed on the block and the curved ends of the crystal were flattened against the block. The center of the crystal was then pushed down so that it touched the backing block near the hole. The atmospheric pressure then held the crystal in position while its periphery was sealed to the block with beeswax, w (Fig. VII-2.2). After about two minutes, the crystal and block were in such intimate contact everywhere that only one or two interference fringes of sodium "D" light were visible over most of the interface, except at a few points where minute dust particles raised small mounds a few wave-lengths high. Several attempts were made before we succeeded in removing all of the dust particles. When good contact was finally obtained everywhere, the copper tube on the back was pinched off and its end was painted with beeswax. (The contact of crystal to backing remained unchanged for six months after the seals were made, at which time we removed the crystal for further testing.)

The crystal backing block was then mounted on a simple swivel arrangement made with two short pieces of angle iron, a (Fig. VII-2.3), ground smooth and connected by single 3/8 inch bolts, d, at each movable

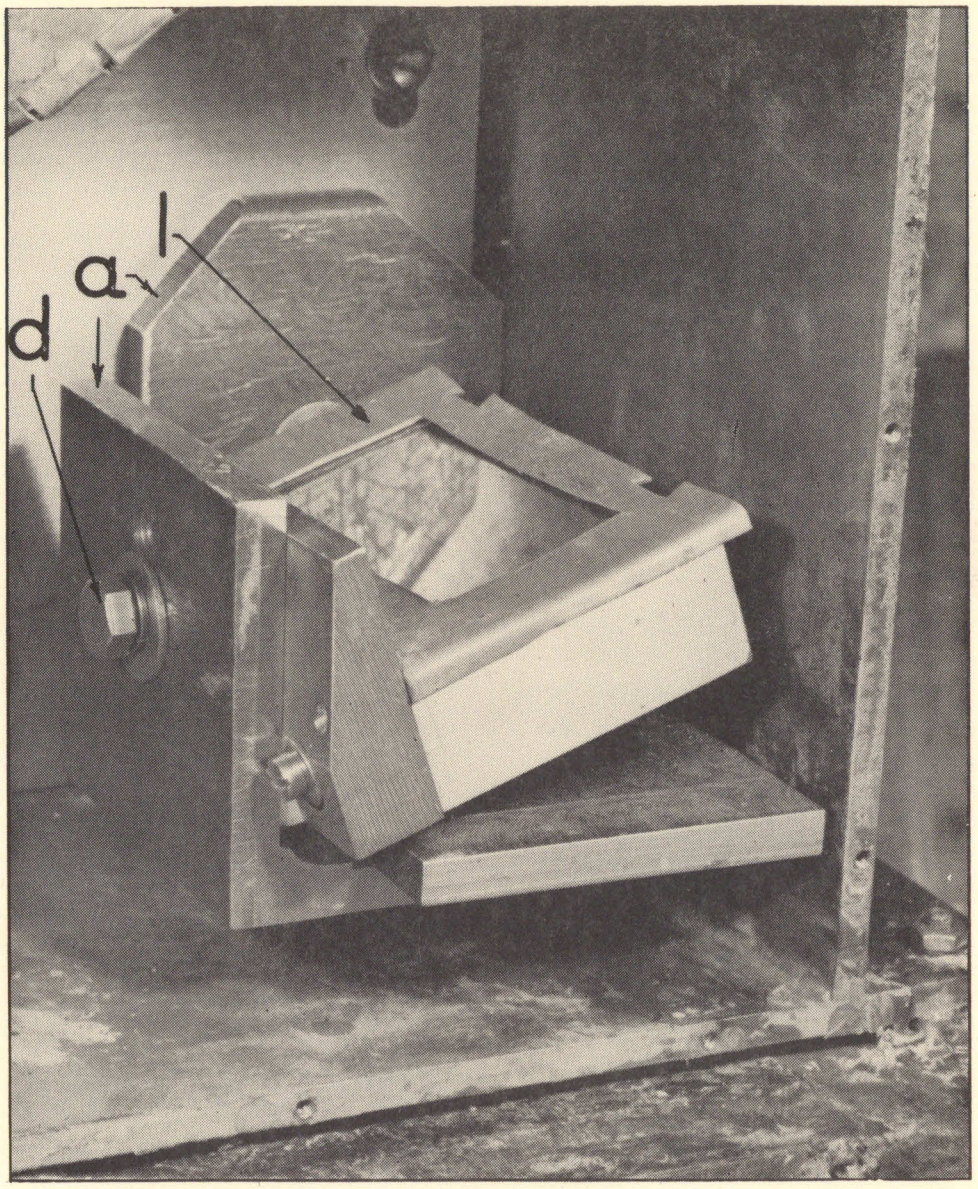

Fig. VII - 2.3. The swivel mounting for the doubly curved crystal.
a = angle iron supports. d = one of the three bolts which are used as axes of rotation.
l = lead shielding to reduce scattered X-rays.

interface, with lock washers and flat washers under them so that the surfaces so bolted together could be rotated around the axis of the bolt to the desired orientation. The bolts were tightened enough to hold the orientation without making the joint too stiff for adjustment.

This swivel arrangement was then mounted in a steel box, B (Fig. VII-2.4), one side, D, of which was removable. Two 3-inch I.D. steel tubes had been welded in the box through holes in the top at orientations such that the beam of x-rays would pass down the first tube, 1, and out along the center of the second tube, 2. The second tube was made vertical in order that the samples could be mounted horizontally and still be normal to the converging x-ray beam. With this arrangement, liquid or powdered samples would flow or shake out to a layer of uniform thickness without the necessity of confining them between two membranes. The sample holder, S, and film holder, F, were mounted on a single unit which could be easily dropped into place or removed from the vertical tube. The film position was fixed relative to the crystal, but the sample holder could slide up or down on two parallel vertical steel rods, R, on the unit, in order to change the size of the diffraction pattern on the film.

The x-ray tube, X, was fastened to an adjustable mount attached to tube 1, and its window was placed directly above a thin aluminum window, A, in the end of that tube. The position of this window was also adjustable. The various lead pinhole apertures used to adjust the resolution of the instrument were placed between the x-ray tube window and the thin aluminum window.

The crystal and x-ray tube were then aligned so that the

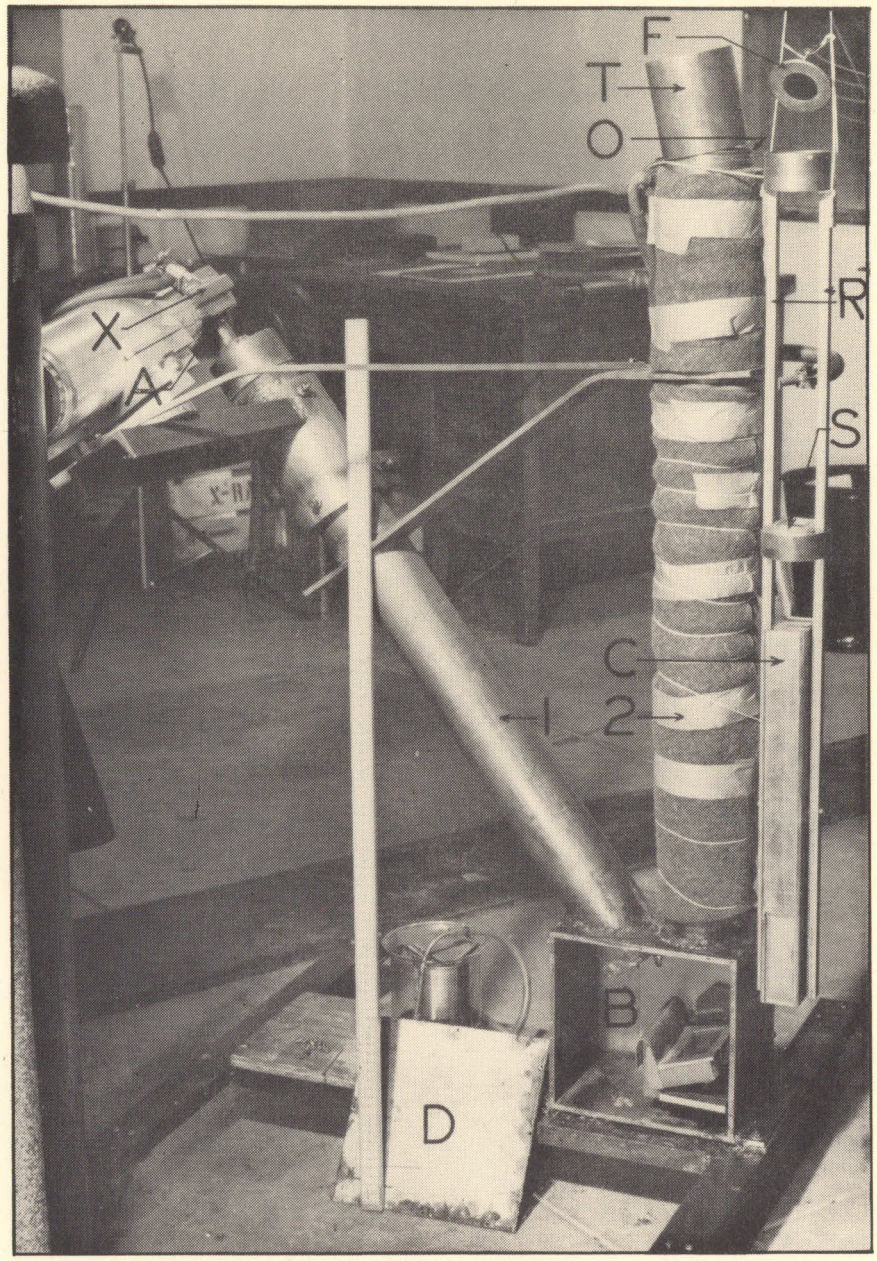

Fig. VII - 2.4. General view of the point focusing monochromator for low angle diffraction studies.

X = X-ray tube (General Electric CA-7 copper target diffraction tube).
A = adjustable aluminum window in tube 1.
B = steel box
D = removable side of box
C = multiple partition baffle system
S = sample holder
R = vertical rods
F = film holder
T = removable cover
O = O-ring
1 = first tube
2 = second tube

copper $K\alpha_1$ radiation was focused up the center of the vertical tube. A photomultiplier tube with zinc sulfide over its window was used to measure the position and intensity of the beam.

Final trimming of the focus, to eliminate astigmatism and to find the position of the best focus, was accomplished using x-ray photographic film. Fig. VII-2.5, which appears on the same page with Figs. VII-3.1 and VII-3.2, shows the image point using an 0.45 millimeter circular aperture at the first focus, p_1, of the crystal. There was still a slight amount of astigmatism in the image, but the alignment was considered satisfactory.

When the alignment was concluded, the side of the box was bolted on and all holes and cracks were sealed with beeswax, so that when the lid, t (Fig. VII-2.4) was slid down over the O-ring fitting, O, the whole system could be filled with helium at slightly above atmospheric pressure. Helium absorbs a negligible fraction of the beam along its two-meter path, whereas air in the same path absorbs about 91.5 percent of the beam.

3. The Converging Multiple Partition Baffle System

When the monochromator was completed, it was found that in extremely long exposures there was an almost circularly symmetrical halo around the focal spot (Fig. VII-3.1). This halo, though far weaker than the primary focus of the x-ray beam, was sufficiently intense to interfere seriously with the observation of the weak diffraction patterns from many interesting biological materials such as

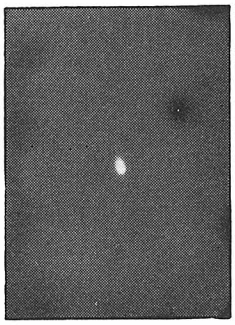

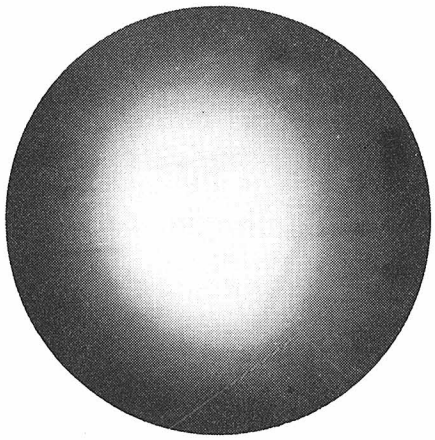

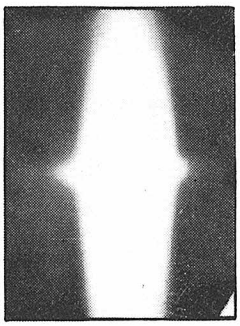

VII - 2.5

VII - 3.1

VII - 3.2

Fig. VII - 2.5. A one-second exposure, through air atmosphere, of the image of an aperture 0.45 mm in diameter, produced by the point focusing monochromator. Note the slight astigmatism that remains. Magnified 2x.

Fig. VII - 3.1. A 20.1 hour exposure, through helium atmosphere, of the same image, showing halo with narrow "light lines," which appear as darker lines in this print of the film. Magnified 2x.

Fig. VII - 3.2. A 20 hour exposure, through helium atmosphere, of the image of an aperture 1 mm in diameter, with the baffle system in place. Note the absence of halo except in the band where the baffle is ineffective, and in the two small projections near the center. Magnified 2x.

The x-ray tube was run at 35 KV. and 20 ma. in all three exposures.

haemoglobin and virus suspensions. The cause of this halo is not definitely known, but various hypotheses as to its origin will be discussed in the next part.

In order to eliminate this halo, a converging multiple partition baffle system somewhat like the ones used in curved-crystal γ-ray spectrometers (19) was placed between the bent crystal and the sample in the converging beam. The baffle plates were 35 cm. long, and were mounted so as to converge toward a line through the point focus. The baffle system was at first attached to the lower end of the rods on the sample and film holder assembly so that it could be easily removed, and it fitted snugly in the vertical tube so that once the crystal was aligned with it, no readjustment was supposed to be necessary. This arrangement is shown in Fig. VII-2.4. The baffle system has since been attached directly to the inside of the vertical tube with adjusting screws, since it was inconvenient to remove it with the sample, and it did not always go back into the proper orientation when replaced.

The baffle system was made by sawing nineteen converging slots about 2 mm. deep in each of two 3-inch strips of brass $\frac{1}{4}$ inch thick and 40 cm. long, using a very thin circular blade on a milling machine. The edges of these two strips were bolted onto two narrower pieces of the same material so as to form a rectangular tube. A strip of rolled lead about 0.5 mm. thick was then slid down the tube between each pair of slots from one end of the tube. The upper ends of these lead strips may be seen in the end of the tube, c, in Fig. VII-2.4. They run in a

direction roughly parallel with the plane of the figure.

The use of the baffle system eliminated the halo entirely, as far as we were able to detect in long exposures, except along a band about 6 mm. wide and in a narrow line vertical to this band through the focal spot. The 6 mm. band represents the limit of resolution of the baffle system, while the narrow line is probably caused by reflection of the main converging beam at very low angles from the surfaces of the lead sheets in the baffle system. Fig. VII-3.2 shows this remaining background.

The most interesting details in the materials we have studied thus far give diffraction effects which fall outside the area not shielded by the baffles. However, if it were necessary, a much narrower band of background could be obtained by using a similar baffle system with two or three times as many slots over the same angular range, and using thin tungsten, or perhaps iron, baffles, which would remain more nearly plane when inserted in the slots.

It may be noticed in Fig. VII-2.4 that the second tube, (2), is covered with thick felt. Under this felt there is a coil of quarter-inch copper tubing, through which we run refrigerated water in order to cool those biological samples that might decompose during an experiment at room temperature.

The inside of the tube and the sample may be kept at a temperature of about five to eight degrees centigrade with this cooling system.

VIII EXPERIMENTAL DETERMINATION OF THE REFLECTION COEFFICIENT

As a check on the intensity equations (Eqs. VI-1.9, VI-1.12, VI-1.13), we have experimentally measured the reflection coefficient.

The reflection coefficient, ρ (Eq. VI-1.13), is the ratio of the amount of flux per unit solid angle incident upon the crystal to the amount reflected toward the focal spot, where only the flux in the spectral line to be focused is counted in the incident flux.

A photomultiplier tube with a layer of zinc sulfide powder spread over the light-sensitive area was used to measure intensities. The tube was wrapped in thin black paper and attached to an amplifier and ammeter. Although the response of this detecting system was not an exactly linear function of incident x-ray flux over a large range of values, the nonlinearity was found to be negligible in the region we used. The effective source was a circular aperture, 0.38 mm. in diameter, placed in front of the x-ray tube focal spot. The intensity of the direct incident beam was measured after it passed through a sheet of nickel foil with an absorption ratio of $(104)^{-1}$ for copper $K\alpha_1$ radiation, as calculated from its mass per unit area, using tables of absorption coefficients in Compton and Allison (15). No filter was used when measuring the intensity of the reflected beam.

Since the K absorption edge of nickel falls between the copper $K\alpha$ and copper $K\beta$ series, the $K\beta$ lines are almost completely absorbed by the filter. Furthermore, with such a thick filter, background and line radiation of longer wave-length than the copper $K\alpha$ doublet are also negligible. Hence, with the filter, the only appreciable

contribution to the incident beam, other than the copper K α doublet, was from the high energy end of the continuum. The high energy contribution was not negligible because the tube had to be run at nearly three times the excitation potential for K-radiation in order to obtain sufficient K α radiation for accurate intensity measurements. The contribution of the high energy part of the continuum was found by the balanced filter method, as follows: The incident radiation intensity was measured after passing it through an iron filter with the same absorption ratio for x-rays in the 20 to 30 kilovolts range as that of the nickel filter. Since iron has its K absorption edge at a longer wave-length than copper, we could assume that the difference between the two measured values of x-ray flux was due almost entirely to x-radiation of wave-lengths between the nickel K-edge and the iron K-edge, which is almost all copper K α radiation when the x-ray tube is run at more than about fifteen kilovolts. The final tests were made at twenty kilovolts.

All measurements of x-ray flux density were made at a distance of 10 cm. from the crystal, in air, so that a correction was made on the measured intensity of the reflected beam for absorption by 20 cm. of air. By applying this correction, subtracting the contribution of the high energy x-rays, and multiplying the incident beam reading by 104, the reciprocal of the absorption ratio of the nickel, we obtained a quotient of 0.0183 for reflected K α flux density divided by the incident K α flux density. However, since the K α_2 line contributes one third of the K α radiation, and since we have chosen

to omit it in the definition of the reflection coefficient, we obtain the following value for ρ:

$$\rho = .0278 \qquad \text{(VIII-1.1)}$$

This value is 1.67 times the value obtained in Table VI-3.2. The difference is probably due to imperfections in the crystal lattice structure caused either by bending the crystal, as suggested by Lind, West, and DuMond (13), or by sawing, grinding, and polishing it.

Since the calculated reflection coefficient of the 023 planes is much larger than even the measured value of reflection of the 052 planes, it is probable that unless the lattice structure is more disrupted with the 023 planes, the reflection coefficient of the 023 planes will be nearer to the calculated value than that of the 052 planes. Exact calculation of the effect of irregularities in crystal lattice structure is impossible without knowing the angular distribution and size distribution of the irregularities.

IX COMPARISON OF THE CRYSTAL MONOCHROMATOR WITH A PINHOLE COLLIMATOR

Since the single crystal monochromator was designed as an improvement over pinhole collimation and filtering, let us compare its performance with that of a pinhole collimator.

Clearly, using pinhole collimation, there is no hope of approaching the monochromaticity obtained with the present doubly focusing crystal diffraction method. However, the Kα doublet can be obtained in fairly pure form, with some sacrifice in intensity, by using filters.

Suppose it were possible to illuminate a pinhole with pure $K\alpha_1$ radiation with no intensity loss. Further suppose the source were a microfocus tube so that only one pinhole would be needed. Then, in order to get a resolution corresponding to a circle 0.5 mm. in diameter at a distance of 40 cm. from the pinhole, the latter would have to have a diameter of 0.25×10^{-3} times the distance from the source in meters. The solid angle $= \frac{\pi d^2}{4R} = 1.23 \times 10^{-7}$. If the size of the source itself were comparable to that of the pinhole, the effective solid angle would be even smaller.

In the first single quartz crystal point focusing monochromator, the measured resolution is sufficient to give an image of about 0.5 mm. in diameter from a point source. The crystal is 3.5 by 7 cm., θ is $71^\circ\ 42'$, and the measured reflection coefficient is 2.78 percent. The converging beam is one meter long. From these data we find that the flux through the focus is equal to the total $K\alpha_1$ radiation that would pass through an aperture subtending a solid angle of 6.61×10^{-5} sterradians from the source. However, with the baffle system in place, about half of the beam is blocked out, and the remaining usable length of the converging beam is only 42 cm. long. Still, the equivalent aperture is 6.0×10^{-6} sterradians, which is 49 times as large as the aperture of the above described idealized pinhole geometry, and probably more than 200 times that of a practical pinhole design with filters. By using a shorter and more accurate baffle system, a larger crystal or smaller values of R, and the 023 Bragg planes rather than the 052, it seems reasonable, from the figures in Table VII-1.1, to expect an increase by a factor of at least ten in the equivalent aperture with

no loss in resolution.

The principal disadvantage of the new instrument, as compared with a pinhole collimator, comes from the requirement that the sample should have an area as large as the cross section of the beam at the sample position. This is a practical disadvantage when one is working with certain biological materials, such as viruses, where it may take several days or weeks to prepare a few milligrams of sample.

X CAUSE OF BACKGROUND

1. Invalid Hypotheses

Several hypotheses as to what contributes the major part of the halo of background around the focal spot, which appears even in the absence of diffracting sample, may be rather definitely rejected on the basis of the intensity distribution of the halo. (See Fig. VII-3.1) This halo is very much less intense than the primary part of the beam which forms the focal spot. At a radius of 1 millimeter from the center of the focal spot, the flux density is approximately 5×10^{-5} times as great as at the focal spot. At 5 millimeters, it is about 2×10^{-6} times as great. Even though these ratios are extremely small, the halo offers serious competition to the diffraction patterns from many interesting sample materials, and makes the baffle system essential in testing those materials.

If incoherent scattering from any of the matter in the path of the beam, including the doubly focusing crystal, gave a major contribution, the halo would not be so much more intense near the focal spot than it is farther out on the detecting film.

If coherent scattering from appreciably disoriented regions or crystallites in the crystal itself were important, one should expect to see a more intense halo in the Y direction from the focus than in the direction normal to Y and to R, since the $K\alpha_1$ line should be resolved into a line by the various parts of the crystal, as in an x-ray crystal powder diagram. There is no evidence of such a tendency in photographs of the halo with any length or intensity of exposure.

The halo cannot be attributed to coherent scattering of parts of the spectrum other than the $K\alpha_1$ line, since reflection of any wavelength must be essentially specular in direction and we have just shown that disorientation of parts of the crystal is negligible. The approximate circular symmetry of the halo is also evidence against this hypothesis.

Careful examination of several photographic images of the halo revealed that it was traversed by some very narrow lines of decreased halo intensity; passing near the central focal spot but not exactly through it. These lines will be called light lines, although they appear dark on the print shown in Fig. VII-3.1.

If the halo were caused by coherent scattering at low angles from the gas in the path of the beam, these light lines would not be explained. Moreover, if this were a major cause, one would expect a decrease in intensity of the halo, relative to that of the focal spot, when helium is substituted for air in the path of the beam. Such an effect has not been observed.

2. A Possible Explanation

The lines in the halo seem to indicate quite definitely that

the halo originates primarily from the bent crystal itself.

The following characteristics of the halo were revealed by further experimentation.

The widths of the light lines were independent of the size or position of the source.

When the source is moved away from the correct position for focusing the $K\alpha_1$ x-ray line and nearly to the correct position for focusing the $K\alpha_2$ line with the crystal, the light lines become much less pronounced, but appear to become doublets.

When the crystal was rotated by 180 degrees about its X axis, the light lines could no longer be found, and faint dark lines were observed at different orientations and positions relative to the focal spot. These dark lines also seemed to be fixed in width and position by the crystal itself, rather than by the source.

Half of the crystal was etched in 25 percent hydrofluoric acid solution for five minutes, until the surfaces of that half appeared definitely less polished than the other half. The crystal was remounted and pictures of the halo from each half were taken with equal exposure times, covering first one half and then the other with lead. No difference in intensity of the halo or of the lines in the halo could be observed, and the lines in the halo remained the same width. Hence, the lines and halo are apparently not related to the irregularities at the crystal surface caused by polishing the crystal.

We may now suggest an explanation for the halo that is consistent with all the experiments performed thus far.

Suppose that when the crystal is bent, there are certain surfaces within the crystal along which the regular periodicity of

the crystal lattice structure is disturbed.* Then x-rays being reflected in the region of one of these irregular surfaces would show diffraction effects due to the fact that the number of Fresnel zones for specular reflection by the crystal planes in that region is reduced. The superposition of these diffraction patterns of varying sizes from different parts of the crystal would give a halo of decreasing intensity outward from the geometrical focal spot, as is observed.

Such a disturbance of the crystal would also give an increased reflection coefficient over that calculated for a perfect crystal, which is consistent with experiment.

It seems clear from the foregoing that the halo must consist of characteristic line radiations almost exclusively. Hence, the light and dark lines in the halo may be attributed to Bragg reflection of certain parts of the halo before they have emerged from the crystal. This reflection would occur from Bragg planes other than the ones contemplated in the design. The narrowness of the lines and the closeness of the doublets observed in the halo indicates that the Bragg angle of the planes causing the lines and doublets must be only a few degrees. Their width is not inconsistent with the hypothesis that the 011 planes

---

* It should be noted that whatever disturbances are introduced in the lattice structure of crystalline quartz by bending must be of a completely reversible nature. This is indicated by the extremely minute elastic loss experienced by quartz oscillators, and also by the fact that when a lamina of quartz is allowed to spring back after being bent, its diffraction properties for x-rays are the same as they were before it was bent. This makes it difficult to invent a mechanism for the formation of disturbances appropriate to explain the changes in x-ray diffraction properties of the crystal introduced by bending the crystal.

are causing them, and the high structure factor of those planes would help to explain the prominence of the lines in the halo. We have not, as yet, had an opportunity to test a fragment of the curved lamina with an x-ray goniometer to see which Bragg planes are correctly oriented to produce the lines in the halo.

XI APPLICATIONS OF THE POINT FOCUSING MONOCHROMATOR IN LOW ANGLE DIFFRACTION

1. Human Haemoglobin

The idea of the new point focusing monochromator was conceived during a series of experiments on low angle diffraction from human haemoglobin, using a slightly revised version of the two crystal point-focusing monochromator constructed by Shenfil and Danielson (11). The instrument was altered to use the 023 planes of quartz instead of the 310 planes in order to obtain higher intensity. The experiment with the two crystal instrument showed very little promise, as exposure times of the order of two to ten days were required to show even the characteristic shoulder on the central maximum in the diffraction pattern of haemoglobin. Meanwhile, the sample usually decomposed. When the new instrument was completed, it was found that patterns could be obtained out to the fourth or fifth subsidiary maximum in 24 hours, using similar samples and the same source; a General Electric CA-7 x-ray diffraction tube with copper target, run at 35 kilovolts and 20 milliamperes, but using a larger aperture in front of the x-ray tube and a larger solid angle of beam than was possible with the two-crystal instrument.

The samples used were whole red cells which were citrated, washed in isotonic saline solution, centrifuged, and reduced with CO_2 or other reducing agents. The samples were about 1mm. thick and consisted of about forty percent cells and sixty percent saline solution. All exposures with blood were made at ordinary room temperatures.

When the distance from the sample to the film was 42.2 cm., the shoulder on the central maximum had a radius of about 1.15 cm. (Fig. XI-1.1a). The structure of the central diffraction pattern is clearly too diffuse to warrant using a smaller aperture than 1 mm. and longer exposure times.

Fig. XI-1.1b is an exposure of the same sample under the same conditions, except that the sample-to-film distance is only 10 cm. (We believe this is the first x-ray diffraction pattern of any type of haemoglobin solution which shows definite single-particle diffraction rings of higher than second order.) Since higher order rings are less affected by interparticle interference than lower ones, we may make a fairly accurate measurement of the mean radius of the single freely suspended haemoglobin molecules, assuming that they are nearly spherical, by measuring high order rings in this figure.

The variable term in the formula for coherent scattering from a sphere of uniform electron density is $J^2_{3/2}(2\pi r/\lambda)/(2\pi r/\lambda)^3$. The maxima of this function for various orders are at the scattering angles (2θ) given in Table XI-1.1. These values, together with the actual angles of the maxima measured from the pattern shown in Fig. XI-1.1b, were used to calculate an experimental value for the mean radius of the human haemoglobin molecule.

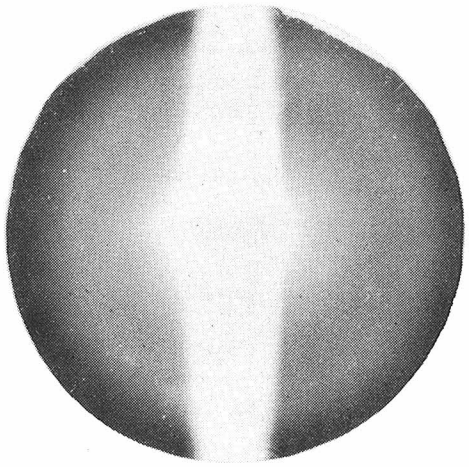

XI - 1.1a

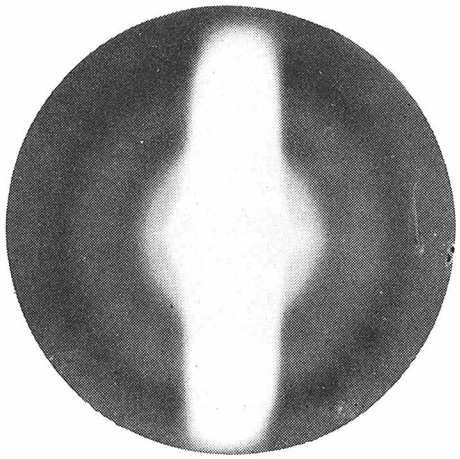

XI - 1.1b

Fig. XI - 1.1a. Diffraction pattern from normal haemoglobin. Sample-to-film distance = 42.2 cm. Exposure 21.5 hrs. at 35 KV, 20 ma, in helium atmosphere, with circular aperture 1 mm in diameter. Magnified 2x.

Fig. XI - 1.1b. Same as a, but sample-to-film distance = 10.0 cm.

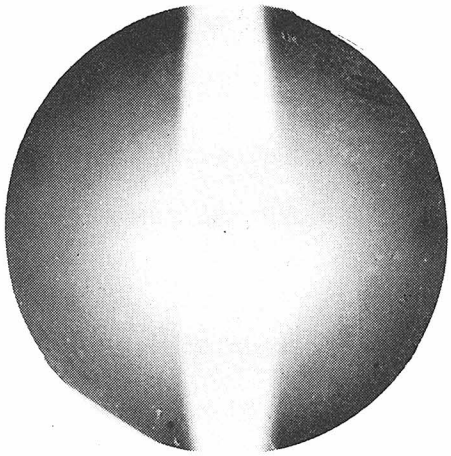

XI - 1.2a

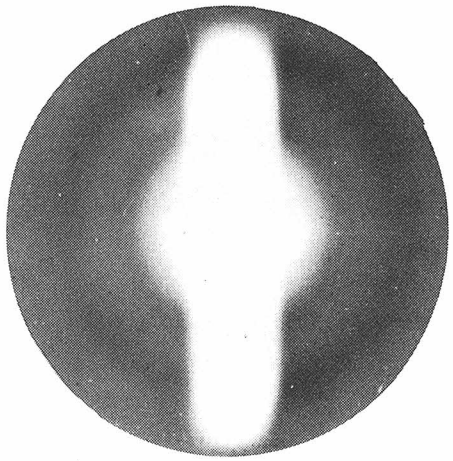

XI - 1.2b

Fig. XI - 1.2a. Diffraction pattern from sickle-cell haemoglobin. Sample-to-film distance = 42.0 cm. Exposure 23.2 hrs. at 35 KV., 20 ma, in helium atmosphere, with no aperture in front of x-ray tube. Intensity of beam is about 1.6 times as great as with the 1 mm aperture. Focal spot of x-ray tube is a rectangle with a projected area of about 1 mm. by 1.5 mm. Magnified 2x.

Fig. XI - 1.2b. Same as a, but sample-to-film distance = 10.0 cm.

Table XI-1.1 Measurements on Human Haemoglobin

Order	Calculated Scattering Angle (2θ) for Maxima	Measured Angle (± .005)	Experimental Mean Radius (r) (λ = 1.54 Å)
1	0.925 λ/r	0.050	28.5 ± 3 Å
2	1.45 λ/r	0.089	25.1 ± 2 Å
3	1.97 λ/r	0.124	24.5 ± 1 Å
4	2.48 λ/r	0.160	23.9 ± 1 Å

The values of the apparent mean radius of the molecules are not in good accord with any average of the values 26.5, 26.5, and 35.5 Å obtained by Bragg, Howells, and Perutz (23) from crystal diffraction studies for the three principal radii of one molecule of haemoglobin on the assumption that it is an ellipsoid of uniform electron density.

It seems unlikely that horse haemoglobin differs greatly in overall shape from human haemoglobin. However, the human haemoglobin molecules may be somewhat smaller, or the outer part of the molecules may have a mean electron density nearer to that of the solvent than the centers.

More information as to the structure of human haemoglobin might be obtained by careful measurements of still higher order diffraction rings, but diffraction angles become rather large for this instrument at higher orders.

The purpose of the earlier experiments with the two quartz crystal instrument was to search for a difference between the diffraction patterns of normal haemoglobin and reduced haemoglobin from

victims of sickle-cell anemia.* Dervichian, Fournet, Guinier, and Ponder (20) have reported some low-angle x-ray diffraction studies in which they found that the first diffraction shoulder on the sickle-cell haemoglobin pattern was less pronounced than that on the normal haemoglobin pattern. With the new instrument we were able to confirm their report quite definitely (cf Fig. XI-1.1a and Fig. XI-1.2a). The diffraction pattern of sickle-cell haemoglobin is very similar to those obtained from dilute suspensions of normal haemoglobin by Riley and Herbert (21). (Riley and Herbert diluted the haemoglobin for their experiments by washing normal cells in somewhat hypotonic saline solutions, which caused the red cells to swell.) The experiments of Riley and Herbert show that the first diffraction shoulder is due mainly to an interparticle interference effect, since it changes with the concentration of the suspended molecules.

However, at our request Dr. M. Murayama, of the Department of Chemistry at the California Institute of Technology, obtained measurements of the haemoglobin concentration in red cells of sickle-cell anemia patients. There appears to be no haemoglobin deficiency as compared with normal red cells.

Furthermore, Perutz and Mitcheson (22) have shown that sickled cells and reduced sickle-cell haemoglobin are birefringent to visible light at ordinary room temperatures whereas normal cells or

---

* Sickle-cell anemia is a hereditary molecular disease of the haemoglobin in red blood cells. In venous blood, where it is in reduced form, many of the red cells become misshapen, often in crescent or sickle form. The misshapen cells are rigid and sometimes form "log-jams" in the veins of the legs, causing ulcerations.

oxidized sickle-cells are not. Hence, reduced sickle-cell haemoglobin must be in a more nearly crystalline state than ordinary haemoglobin at normal concentration. One would therefore expect more rather than less interparticle interference with sickle-cell haemoglobin. At present there is no very satisfactory explanation for this apparent anomaly.

Fig. XI-1.2b is a pattern from the same sample of sickle-cell blood taken with a 10 cm. sample-to-film distance, so that several higher order diffraction rings appear. In this pattern there appears to be no difference between sickle-cell and normal blood (cf. Fig. XI-1.1b) except that the exposure required for the sickle-cell pattern was somewhat greater, which could be due to a difference in the total amount of haemoglobin in the two samples. Hence, we conclude that although sickle-cell and normal haemoglobin aggregate differently, the individual molecules must be of almost identical structure.

2. Southern Bean Mosaic Virus

Although the experiments with haemoglobin do indicate the improvement in intensity over the old instrument with two curved crystals in tandem, they do not really show its advantage over pinhole collimation and filtering for very low angle work. Much more gratifying results are now being obtained by Dr. Donald Caspar, a visiting Research Fellow from Yale, who has used the instrument to measure Southern Bean Mosaic Virus, (S.B.M.V.), and various other approximately spherical biological samples of the order of hundreds of Angstroms in diameter. He is interested in finding whether or not there are large inhomogeneities in electron density distribution within the particles by comparing the intensities and positions of various orders of diffraction maxima and minima when the cells are immersed in media of varying electron densities. His measurements on S.B.M.V. indicate there are none. Fig. XI-2.1, which shows the pattern obtained with a sample of S.B.M.V. at 30 cm. from the film, is an example of his studies with the present instrument.

The exposure time on the sample was 48.1 hours, and a circular aperture of 0.38 mm. diameter was used in front of the x-ray tube. The G.E. CA-7 x-ray tube was run at 35 KV and 20 MA. The sample was about 1 mm. thick and was an aqueous suspension of roughly thirty percent virus concentration. Since this type of virus decomposes rapidly at room temperature, the refrigeration system was used during the exposure.

Measurements of the rings indicate a radius of 143 $\pm$ 1 Angstroms, assuming the particles are spheres of uniform electron density. The

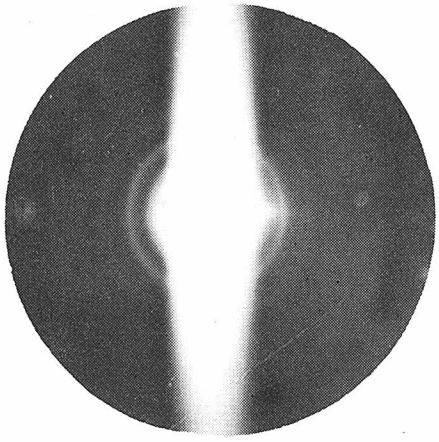

Fig. XI - 2.1. Diffraction pattern from Southern Bean Mosaic Virus. Sample-to-film distance = 30 cm. Magnified 2x.

sharpness of the rings indicates that they are extremely uniform in size and spherical in shape. The following table is a comparison made by Dr. Caspar between the measured and calculated dimensions of the diffraction pattern:

Table XI-2.1 Measurements on S.B.M.V.

Order of Ring	Radius of Ring on Film	2θ (radians) (Sample 30 cm. from film)	Calculated 2θ (assume r = 143 Å)
1	3.14 mm.	$1.05 \times 10^{-2} \pm .01$	0.995×10^{-2}
2	4.76 mm.	$1.59 \times 10^{-2} \pm .01$	1.56×10^{-2}
3	6.38 mm.	$2.13 \times 10^{-2} \pm .01$	2.12×10^{-2}
4	7.88 mm.	$2.63 \times 10^{-2} \pm .02$	2.67×10^{-2}

The large apparent error in the first order subsidiary maximum is undoubtedly due to interparticle interference effects, which probably also account for the fainter ring close to the first order ring. Higher order rings should be changed very little by interparticle interference.

The value of 143 Angstroms agrees exactly with the results obtained by Leonard, Anderegg, Shulman, Kaesberg, and Beeman at the University of Wisconsin (24), using slit collimation and Geiger counter detectors. The maxima are much sharper with the point focus than with the line focus because the diffraction pattern is not smeared along a line as it is with the slit geometry.

REFERENCES

1. W.H. Zachariasen: Theory of X-Ray Diffraction in Crystals, J. Wiley & Sons (1945)
2. W.L. Bragg: Proc. Camb. Phil. Soc. 17, 43 (1912)
3. C.G. Darwin: Phil. Mag. 27, 325; 675 (1914)
4. P.P. Ewald: Ann. d. Phys. 54, 519; 577 (1917)
5. J.W.M. DuMond, H.A. Kirkpatrick: R.S.I. 1, 88 (1930)
6. T. Johansson: Naturwiss. 20, 758 (1932)
7. H.H. Johann: Zeit. f. Physik 69, 185 (1931)
8. J. Despujols: Compt. Rend. 235, 716 (1952)
9. G. Hagg, N. Karlsson: Acta Cryst. 6, 728 (1952)
10. D.W. Berreman, J.W.M. DuMond, P.E. Marmier: R.S.I. 25, 1219 (1954)
11. L. Shenfil, W. Danielson, J.W.M. DuMond: J. App. Phys. 23, 854 (1952)
12. A. Hoyt: Phys. Rev. 40, 477 (1932)
13. D.A. Lind, W.J. West, J.W.M. DuMond: Phys. Rev. 77, 475 (1950)
14. P.H. Wei: Zeit. f. Kryst. 92, 355 (1935)
15. Compton and Allison: Z-Rays in Theory and Experiment, 2nd Ed., Van Nostrand (1935)
16. G. Borrman: Zeits. f. Krist. 106, 2 (1954)
17. W.L. Bond and E.J. Armstrong: Bell Tel. Tech. Journ. 22, 303 (1942)
18. J.W.M. DuMond, D.A. Lind, E.R. Cohen: R.S.I. 18, 617 (1947)
19. J.W.M. DuMond: R.S.I. 18, 626 (1947)
20. D.G. Dervichian, G. Fournet, A. Guinier, E. Ponder: Revue d'Hematologie 7, 567 (1952)
21. D.P. Riley and D. Herbert: Bioch. Bioph. Acta 4, 374 (1950)

REFERENCES

22. M.F. Perutz and J.M. Mitcheson: Nature 166, 677 (1950)

23. W.L. Bragg, E.R. Howells, M.F. Perutz: Proc. Roy. Soc. 222, 33 (1954)

24. B.R. Leonard, J.W. Anderegg, S. Shulman, P. Kaesberg, W.W. Beeman: Bioch. Bioph. Acta 12, 499 (1953)